SIMULATING INTERDECADAL VARIATIONS OF THE THERMOHALINE CIRCULATION BY ASSIMILATING TIME-DEPENDENT SURFACE DATA INTO AN OCEAN CLIMATE MODEL

GUOQING LI

National Library of Canada
Acquisitions and Bibliographic Services Branch
395 Wellington Street
Ottawa, Ontario
K1A 0N4

Bibliothèque nationale du Canada
Direction des acquisitions et des services bibliographiques
395, rue Wellington
Ottawa (Ontario)
K1A 0N4

Your file Votre référence

Our file Notre référence

NOTICE

The quality of this microform is heavily dependent upon the quality of the original thesis submitted for microfilming. Every effort has been made to ensure the highest quality of reproduction possible.

If pages are missing, contact the university which granted the degree.

Some pages may have indistinct print especially if the original pages were typed with a poor typewriter ribbon or if the university sent us an inferior photocopy.

AVIS

La qualité de cette microforme dépend grandement de la qualité de la thèse soumise au microfilmage. Nous avons tout fait pour assurer une qualité supérieure de reproduction.

S'il manque des pages, veuillez communiquer avec l'université qui a conféré le grade.

La qualité d'impression de certaines pages peut laisser à désirer, surtout si les pages originales ont été dactylographiées à l'aide d'un ruban usé ou si l'université nous a fait parvenir une photocopie de qualité inférieure.

Canada

SIMULATING INTERDECADAL VARIATIONS OF THE THERMOHALINE CIRCULATION BY ASSIMILATING TIME-DEPENDENT SURFACE DATA INTO AN OCEAN CLIMATE MODEL

By

©Guoqing Li, B.Sc., M.Sc.

A thesis submitted to the School of Graduate

Studies in partial fulfillment of the

requirements for the degree of

Master of Science

Department of Physics

Memorial University of Newfoundland

February, 1994

St. John's Newfoundland Canada

ISBN 0-315-91640-0

Canada

Abstract

We explore the feasibility of simulating interdecadal variations of the temperature, salinity and thermohaline circulation in the North Atlantic using an ocean general circulation model (OGCM) driven by time-dependent surface data. The natural way to drive the ocean is to use the surface heat and freshwater fluxes. In this thesis, we investigate the alternative of using surface temperature and salinity data since compared to heat and freshwater flux data, they are more accurate and more readily available.

We do the experiments using idealized North Atlantic sized box geometry. In order to obtain a set of interdecadally-varying data, we first reproduced the results described by Zhang, Greatbatch and Lin (1993). Temperature, salinity, surface heat and freshwater flux are output from this control run and serve as "observations" in the further experiments.

We can apply either a restoring boundary condition or a flux boundary condition at the ocean surface. To simulate the interdecadal variations, there are four choices for the surface boundary conditions: i) flux conditions on both temperature and salinity; ii) restoring conditions on both temperature and salinity; iii) a restoring condition on temperature and a flux condition on salinity (mixed boundary conditions); and iv) a

flux condition on temperature and a restoring condition on salinity ("reversed mixed" boundary conditions). The restoring boundary conditions are to be understood in a sense of *data assimilation*.

The experiments show that all the choices work well except mixed boundary conditions. It is found that a correct simulation of the thermohaline circulation is necessary to obtain a correct distribution of the sub-surface variables. Under mixed boundary conditions, a positive feedback between the development of a freshwater cap and heat-loss reduction results in either a collapsed or violent overturning thermohaline circulation quite unlike what happens in the control run. So mixed boundary conditions are not suitable for interdecadal simulation studies. The use of both-restoring boundary conditions does not allow a freshwater cap to develop because the surface salinity is constrained by the use of the restoring condition on salinity. This guarantees a realistic thermohaline circulation and, consequently, a correct distribution of the sub-surface temperature and salinity. In contrast with mixed boundary conditions, "reversed mixed" boundary conditions work well. This is because both surface heat flux and surface salinity are controlled, breaking the positive feedback that occurs under mixed boundary conditions.

A common feature of the successful experiments is that all of them have a correct surface heat flux distribution (prescribed or implied), whereas the surface salt

flux may defer (though not significantly). This shows that whatever the boundary condition is, it is necessary to get the surface heat flux seen by the ocean correct in order to have a realistic thermohaline circulation. It also shows that controlling surface salinity is more important than getting every detail of the freshwater flux correct (fortunately, freshwater flux data are the poorest). The results show that we should use both-restoring boundary conditions or reversed mixed boundary conditions to simulate interdecadal variations of the thermohaline circulation.

Acknowledgements

Since the beginning of my studies in the Physical Oceanography Group at MUN's Physics Department, Dr. Richard Greatbatch, my supervisor, has been providing support, guidance, and encouragement. He is the original thinker and planner of this thesis work and offered continual guidance at every stage of this study. He reviewed the manuscript many times with great patience and gave invaluable suggestions and comments which made a great contribution to the completion of this thesis. For his help, I offer my sincerest thanks.

I would also like to thank Mr. Allan Goulding for his great contribution to the development of the model used in this study, for teaching me the art of wise, efficient computer programming and for his patience when helping me to solve my computer problems. I am also grateful to Dr. Sheng Zhang for many stimulating discussions and valuable suggestions, and particularly for his wit in simplifying some abstruse papers into simple words in my mother-tongue when I found them hard to understand. Thanks to Dr. Wenju Cai we found that our "reversed mixed" boundary conditions were used as early as in Manabe and Stouffer (1988).

I am also indebted to the teachers who brought me to the gate of oceanography and numerical modelling. They are Drs. Alex Hay, Brad de Young, Kevin Lamb and

Michael Rochester at MUN, Prof. Jiping Chao at Institute of Atmopheric Physics, Academia Sinica and Dr. Huiding Wu at Peking University.

I cannot adequately express my gratitude to my wife and my parents for their unrelenting support and encouragement, and to my friends Youyu, Fraser, Liren and Hong for sharing in both the joys and frustrations of my life and study during the last two years.

This work forms part of the Canadian university participation in the World Ocean Circulation Experiment and is supported by the Natural Sciences and Engineering Research Council of Canada through their Collaborative Research Initiative Programme. Supports from MUN's School of Graduate Studies and Department of Physics through Graduate Fellowship and Departmental assistantship are also acknowledged.

Contents

List of Figures

List of Tables

Chapter 1

Introduction

It is well accepted that the thermohaline circulation of the world ocean is to a large degree driven from the North Atlantic through the production of the North Atlantic Deep Water (NADW). As water flows north into the high-latitude North Atlantic, it loses heat to the atmosphere and becomes colder and denser. At a number of sites in the northern North Atlantic in the winter, surface waters become dense enough to convect to depths greater than 1,000 metres. These then spread into the rest of the global ocean as its intermediate and deep waters. This process initiates a worldwide overturning circulation cell on the meridional plane in which northward transport of upper ocean warm water is balanced by deep return flow of cold water (see Fig. 1.1). This overturning circulation is called the thermohaline circulation (THC)

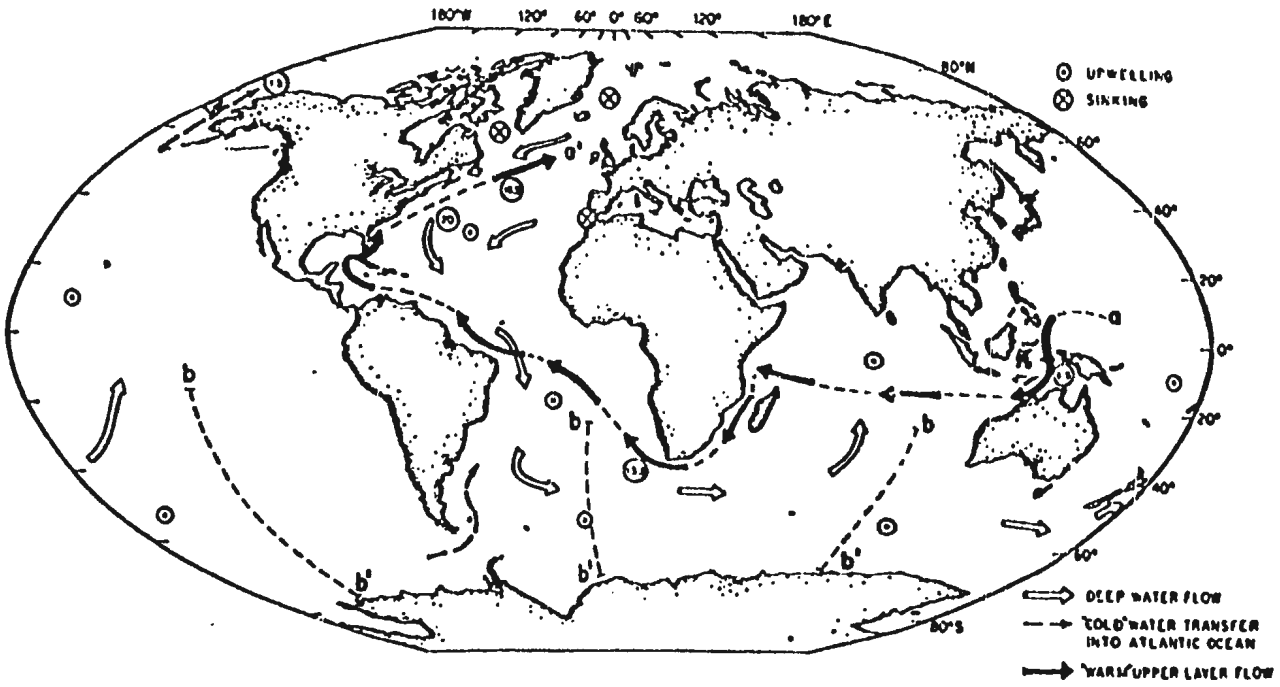

Figure 1.1: Global structure of the thermohaline circulation cell associated with NADW production. The warm water route, shown by the solid arrows, marks the path proposed by Gordon (1986) for return of upper layer water to the northern North Atlantic as is required to maintain continuity with the formation and export of NADW. The circled values are volume flux in $10^6 m^3/s$ which are expected for uniform upwelling of NADW with a production rate of $20 \times 10^6 m^3/s$. These values assume that the return within the cold water route, via the Drake Passage, is of minor significance (adapted from Fig.2a of Gordon, 1986).

(see Gordon, 1986, for a review). It plays an important role in the present-day climate system because it transports a large amount of heat to high latitudes through the upper ocean and loses the heat to the atmosphere through deep water production, resulting in a much warmer climate in high latitude regions than would be the case in the absence of the thermohaline circulation. Therefore changes in the strength of the thermohaline circulation, can have a profound effect on the local climate. At high latitudes, there is always a freshwater flux into the ocean This works as a break to the thermally-driven overturning cell. But in modern climate, the thermal driving is dominant in the North Atlantic. Fig. 1.2 gives the annual average of the ratio of the heat and salt density fluxes.

There is growing evidence to show the importance of decadal variability in the climate system. Ghil and Vautard (1991) have noted the importance of removing the decadal signal from globally averaged surface air temperatures to properly estimate the rate of global warming. The Atlantic Ocean is believed to be of particular importance at the interdecadal time scale and has attracted the most attention (see Gordon *et al.*, 1992, for a review). The idea that decadal fluctuations in sea surface temperature (SST) are linked to ocean circulation was first hypothesized by Bjerknes (1964). The possible role of changes in the thermohaline circulation, and the associated poleward heat transport, is further discussed by Bryan and Stouffer (1991).

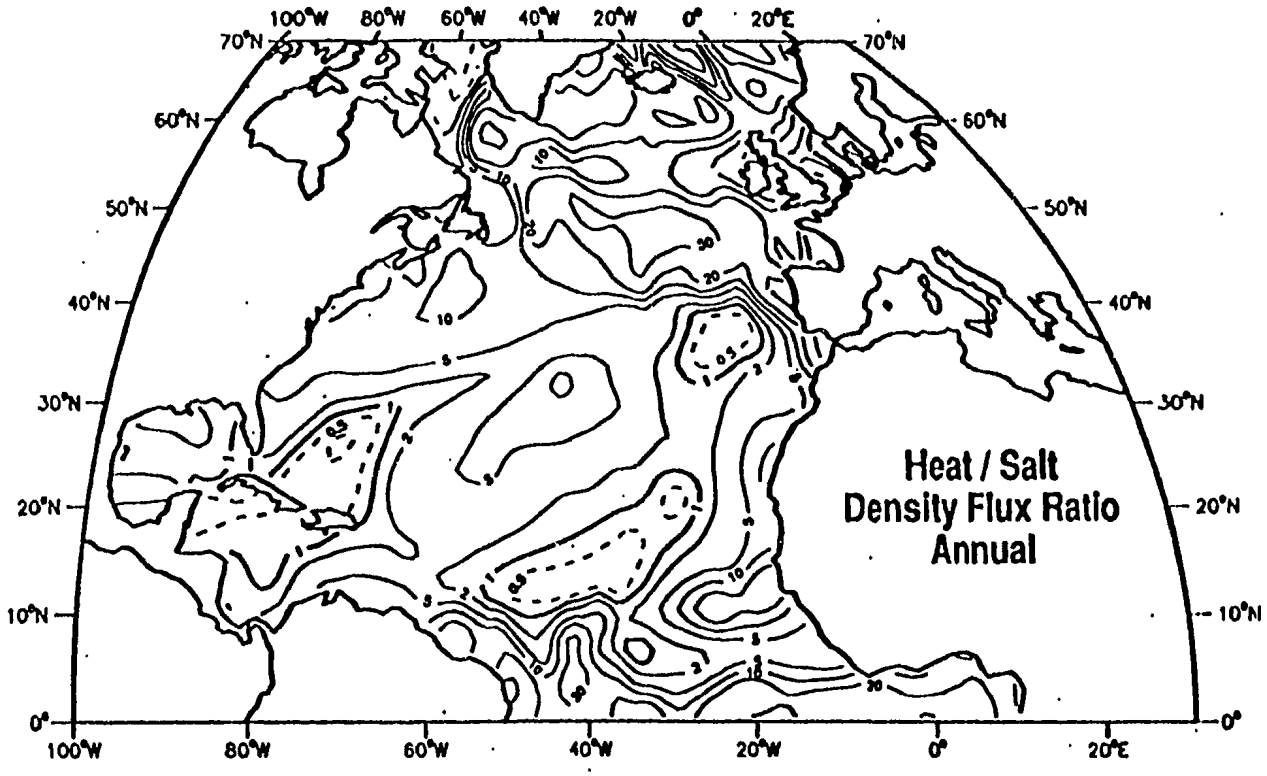

Figure 1.2: The absolute value of the ratio of the heat and salt density fluxes (adapted from Fig.5 of Schmitt *et al.*, 1989).

Kushnir (1993) provides evidence for the view that 30-40 year interdecadal variations in SST are influenced by changes in the ocean circulation. Further evidence for the role of the ocean circulation has been provided by Deser and Blackmon (1993) who suggest that the general warming in North Atlantic SST during the 1920s–30s, followed by a cooling in the 1960s (Fig. 1.3), may have been associated with changes in the Gulf Stream. In particular, they point to the decrease in Gulf Stream transport in the 1970s, compared to the late 1950s, implied by the diagnostic calculations of Greatbatch *et al.* (1991), and supported by the work of Sato and Rossby (1993).

There is also evidence that the subsurface structure of the North Atlantic undergoes decadal variability. By comparing composites for the pentads 1955–59 and 1970–74, Levitus (1989a,b,c) found that the subtropical gyre and the eastern portion of the subarctic gyre (at intermediate depths) of the North Atlantic were colder and fresher during 1970–74 compared to 1955–59 (see Fig. 1.4 and Fig. 1.5). Greatbatch and Xu (1993) have suggested that at 24°N, the poleward heat transport associated with these changes was reduced in the 1970–74 pentad compared to climatology. Read and Gould (1992) have traced subsurface changes in the thermohaline structure of the subpolar North Atlantic. They relate these changes to the cessation of deep water formation in the Labrador Sea in the late 1960s and early 1970s. This was associated with the "Great Salinity Anomaly" (Dickson *et al.*, 1988), and the capping of the wa-

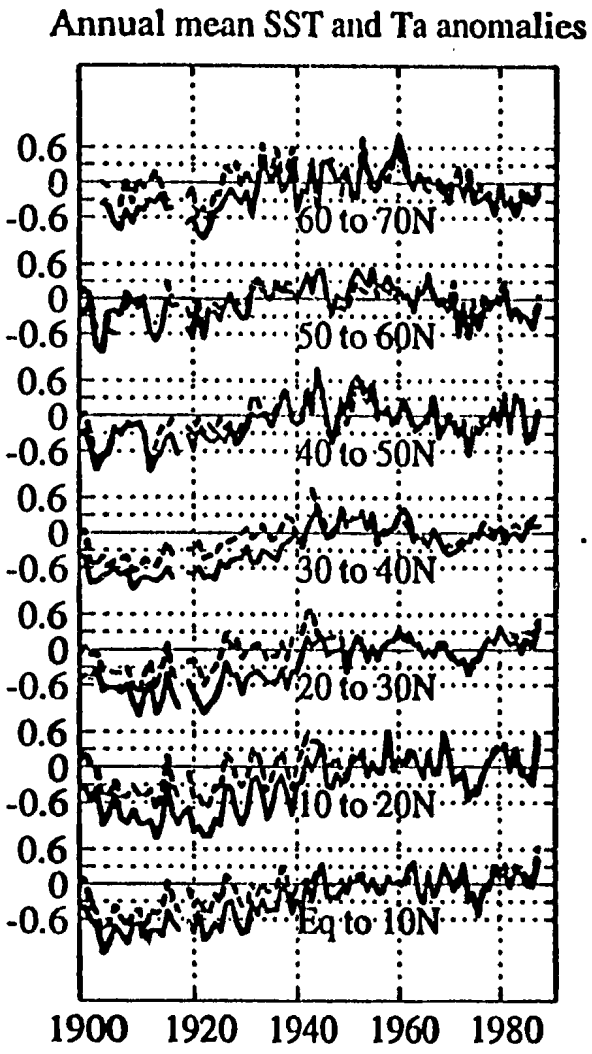

Figure 1.3: Annual mean Atlantic SST (solid), and air temperature (dashed) anomalies averaged in seven 10° latitude belts from the equator to 70°N. Anomalies are calculated with respect to the 1950 to 1979 average. The ordinate is divided into 0.3°C segments (adapted from Fig.2 of Kushnir, 1993).

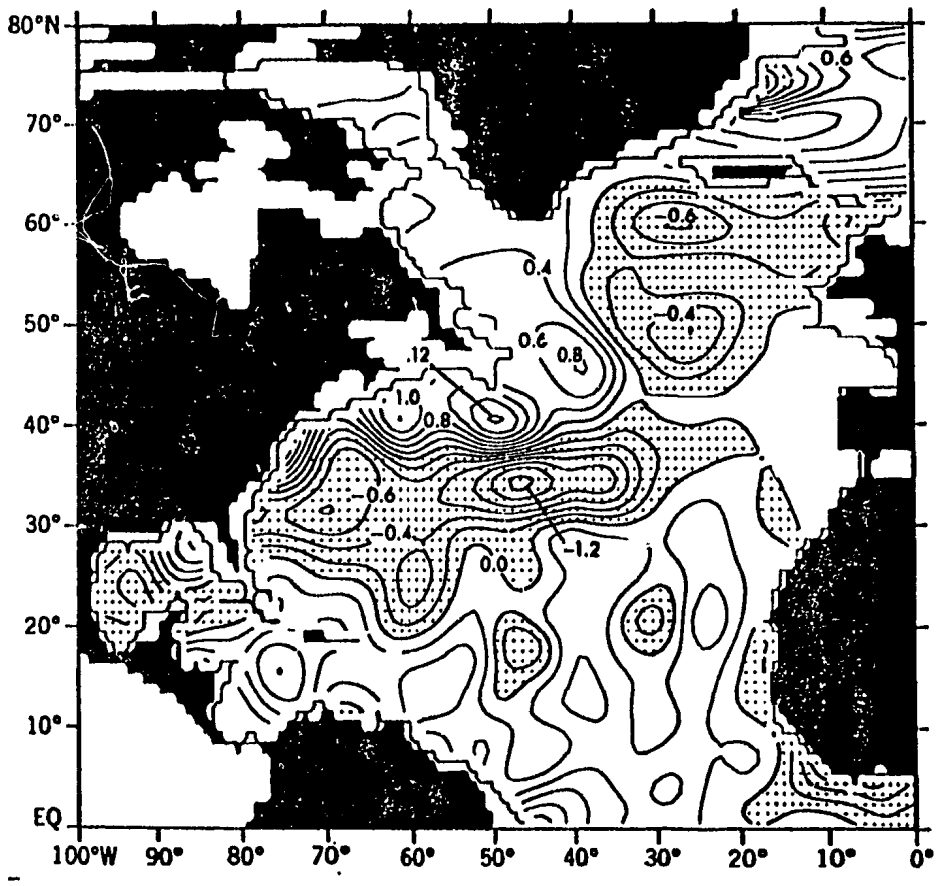

Figure 1.4: Temperature difference (in degree Celsius) for 1970–1974 minus 1955–1959 at 500-m depth. Dot shading indicates negative values. (adapted from Fig.7 of Levitus, 1989a).

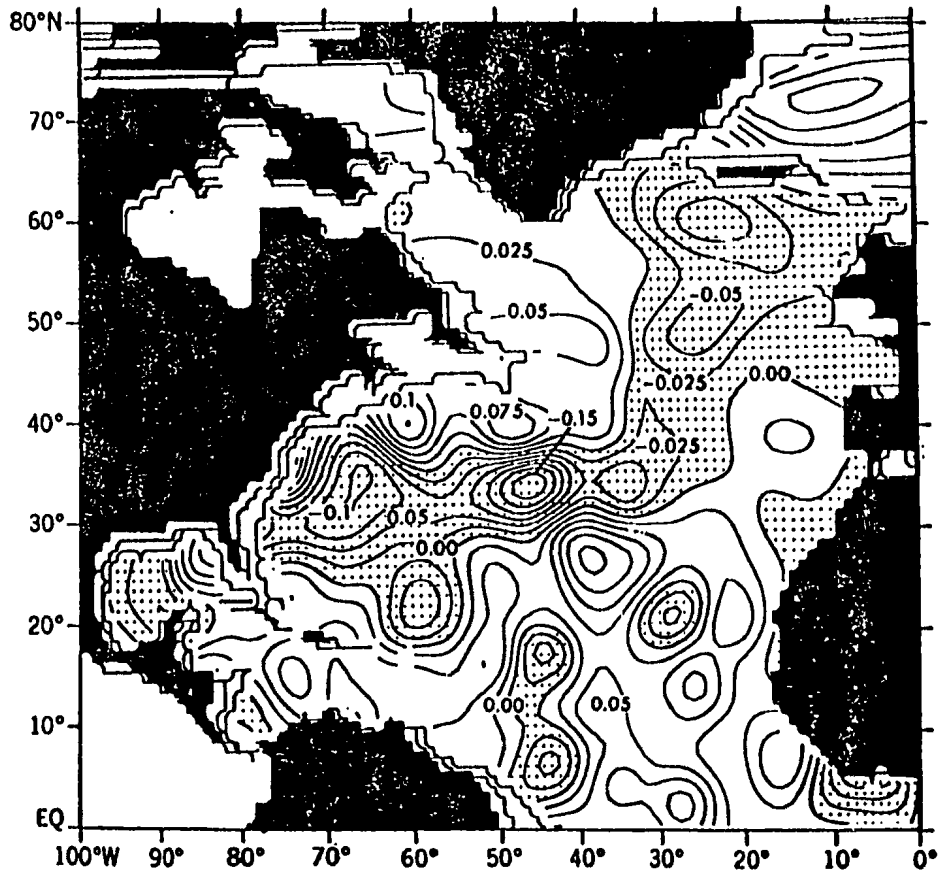

Figure 1.5: Salinity difference for 1970–1974 minus 1955–1959 at 500-m depth. Dot shading indicates negative values. (adapted from Fig.8 of Levitus, 1989a).

ters in the Labrador Sea by anomalously fresh water. For example, based on the data collected at Ocean Weather Ship *Bravo* (56°30′N, 51°00′W) between 1964 and 1974, Lazier (1980) found that near-surface salinity values between 1967 and 1971 were significantly lower than those between 1964–1967 (Fig. 1.6) and coincident with the lower salinity values, the winter-time heat losses were less than normal. He pointed out that the combination of increased stratification with the low heat losses limited the convectively mixed upper layer in winter to unusually shallow depths.

Interdecadal variability has also been found in numerical models. For example, Delworth, Manabe and Stouffer (1993) found interdecadal variations of the North Atlantic thermohaline circulation in a coupled atmosphere-ocean model. Marotzke (1990) and Weaver and Sarachik (1991a,b) have reported decadal and interdecadal oscillations in ocean-only models run under mixed boundary conditions (that is, the use of a restoring boundary condition on the surface temperature and a flux boundary condition on the surface salinity). Zhang, Greatbatch and Lin (1993) (hereafter, referred to as ZGL) have observed interdecadal oscillations in their ocean model run under a boundary condition obtained by coupling the ocean to a zero-heat-capacity atmosphere. Greatbatch and Zhang (1993) recently report an interdecadal oscillation in an ocean-only model forced by a constant surface heat flux.

In this study, we explore the feasibility of simulating interdecadal variations of

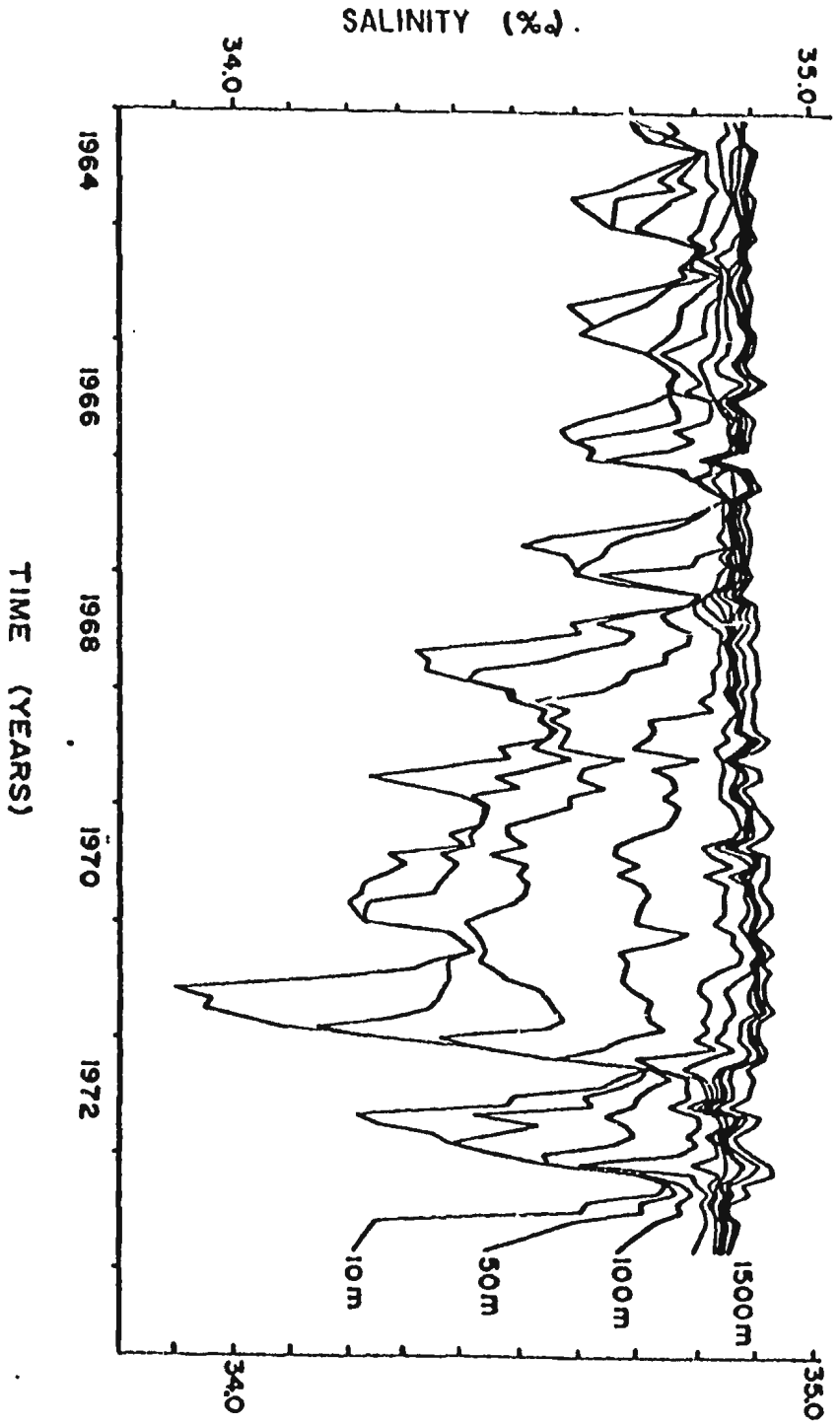

Figure 1.6: Monthly averages of salinity at eleven depths at station *Bravo* (56°30′*N*,51°00′*W*) from 1964 to 1973 (adapted from Fig.2 of Lazier, 1980).

the temperature, salinity and thermohaline circulation in the North Atlantic using an ocean general circulation model (OGCM) driven by time-dependent surface data. We experiment with different kinds of boundary conditions at the ocean surface to test the behavior of the model in order to determine what surface data are appropriate for this purpose. We do this because of a desire to use surface temperature and salinity data, since compared to flux data, they are more accurate and more readily available. The natural way to drive the ocean is to use the surface heat and freshwater fluxes. Unfortunately data on these fluxes are too uncertain and sparse. For example, we still do not have adequate techniques or instruments to measure precipitation over the sea. Clarke (1992) points out, "Over the near future, it would appear that the only possible strategy for estimating the freshwater flux in the North Atlantic is through the coupling of an upper-ocean model with regular measurements of surface and upper-ocean salinity from merchant vessels and moored or drifting profiling instruments, for which suitable devices must be developed quickly." Tziperman and Bryan (1993) have made an effort to estimate the air-sea fluxes by combining the fluxes diagnosed from an ocean model using surface temperature and salinity data, and the fluxes estimated from meteorological ship data.

We do the experiments in an idealized North Atlantic sized box geometry before going on to the complexities of attempting realistic simulations using real data in

future work. To implement the above ideas, we first reproduce ZGL's results. They found that when a zero-heat capacity atmosphere is coupled to the ocean model, a cold, fresh water pool is developed and advected horizontally and vertically by the circulation in high latitudes, showing interdecadal oscillations. The model output of this control run serve as a set of data for our further experiments. This data set is 4-dimensional and contains all model variables including the velocity field. In this control run, the temperature, salinity and thermohaline circulation all show interdecadal oscillations. Hereafter, the sea surface temperature and salinity (SST and SSS) of this data set are referred to as "surface property data", and the heat flux and freshwater flux are referred to as "surface flux data". In the following, "surface data" may mean either SST, SSS or the surface fluxes. To drive the ocean model, we may select either SST or heat-flux to form a surface boundary condition on temperature and select either SSS or salt-flux to form a surface boundary condition on salinity. The ocean model is driven by surface property data through a restoring boundary condition in which the value in the top model level is relaxed to the surface property data with a chosen restoring time of, say, several or tens of days. Under this kind of restoring boundary condition, the surface property of the ocean model (be it SST or SSS) can not depart far from the surface property data to which it is being relaxed. When a flux boundary condition is used, the corresponding surface

property of the ocean model is not constrained (we label it as uncontrolled variable in later discussions). It will be realistic only if the initial value, the flux data, horizontal advection, vertical convection and other dynamics of the model all are correct.

There are four possible choices corresponding to four pairs of surface boundary conditions: i) both-flux boundary conditions, in which the time-dependent heat and freshwater flux data are imposed on the ocean surface; ii) both-restoring boundary conditions, in which temperature and salinity at the top model level are restored to the time-dependent SST and SSS data, respectively; iii) mixed boundary conditions, in which the top-level temperature is restored to the time-dependent SST data, while a flux boundary condition is applied to salinity; and iv) "reversed mixed" boundary conditions, in which the top-level salinity is restored to time-dependent SSS while surface heat flux boundary condition is applied to temperature. It is worth noting here that none of these boundary conditions are "true" boundary conditions except both-flux boundary conditions. In reality, the ocean sees the flux from the air to the ocean. Therefore we should understand the above restoring boundary conditions as a type of *data assimilation*. The surface value of a variable is in effect prescribed (more or less loosely, depending on the restoring time) when a restoring condition is applied and the other variables are taken care of by the use of a surface flux boundary condition and model dynamics. In reality, we would like to use as much

surface property data as possible because of the uncertainty and unavailability of flux data.

To initialize the ocean model, we use the initial value of the data set from the control run at all depths, not just the surface data. In the future, we will have to solve problems such as how to initialize the model with real data before doing real simulation. In this study, we are not going to discuss how to form an initial field. Rather, we test the behavior of the ocean model under different surface boundary conditions.

Since the initial conditions and boundary conditions come from a set of perfect data, naturally we expect the model results will be very close to the data under all the four kinds of boundary conditions. But the results show that all cases work well except the mixed boundary condition case. Mixed boundary conditions (prescribing temperature but using a flux boundary condition on salinity) allows a positive feedback between the formation of a freshwater cap and a reduction in surface heat loss (more explanation is given in Chapter 4). This results in a bias toward either a collapse of the thermohaline circulation or a violent overturning circulation and thus fails to simulate the data. Constraining the surface salinity to approach a prescribed value, as in the both-restoring boundary condition and reversed mixed boundary condition cases, breaks the positive feedback mechanism and leads to a good result in

simulating the thermohaline circulation shown in the data. This bears some analogy to Manabe and Stouffer (1988). They used a restoring condition on salinity (but not on temperature, corresponding to our reversed mixed boundary conditions) to bring the surface salinity close to the modern climate in order to induce a thermohaline circulation in the North Atlantic in their coupled atmosphere-ocean general circulation model. Lack of the North Atlantic thermohaline circulation makes a colder, fresher surface than modern climate because the thermohaline circulation advects warmer, saltier water to high latitudes.

The plan of this thesis is as follows. A Bryan-Cox-Semtner type OGCM developed for use in this study is described in Chapter 2. With this model, in Chapter 3, we reproduce the results described by Zhang, Greatbatch and Lin (1993). Then the model output will serve as data in Chapter 4 to drive the ocean model under different boundary conditions. We give a summary and conclusions in Chapter 5.

Chapter 2

Model Description

2.1 Introduction

Our model is built by basically following Bryan (1969) and Semtner (1974). The governing equations of the model consist of the two horizontal momentum equations (non-linear advection terms ignored), the hydrostatic equation, the continuity equation, tracer equations for temperature and salinity, and a non-linear equation of state. The major simplifications are: the hydrostatic assumption, the Boussinesq assumption with respect to density variations, and a parameterization treatment of mixing process under a "turbulent viscosity" hypothesis.

2.2 Governing Equations

We take the earth to be a sphere of radius a, rotating with angular speed Ω. We write the equations in a spherical coordinate system, with λ, ϕ, and z representing longitude, latitude, and height, respectively. The ocean is set between the surface $z = 0$ and the bottom $z = -H(\lambda, \phi)$. We have seven variables to describe the physical condition of the ocean: three velocities (u, v, w), pressure p, density ρ, temperature T, and salinity S. The governing equations are as follows:

$$\frac{\partial u}{\partial t} - fv = -\frac{1}{\rho_0 a \cos\phi}\frac{\partial p}{\partial \lambda} + F^{\lambda} \tag{2.1}$$

$$\frac{\partial v}{\partial t} + fu = -\frac{1}{\rho_0 a}\frac{\partial p}{\partial \phi} + F^{\phi} \tag{2.2}$$

$$\frac{\partial p}{\partial z} = -\rho g \tag{2.3}$$

$$\frac{1}{a\cos\phi}\frac{\partial u}{\partial \lambda} + \frac{1}{a\cos\phi}\frac{\partial}{\partial \phi}(v\cos\phi) + \frac{\partial w}{\partial z} = 0 \tag{2.4}$$

$$\frac{\partial T}{\partial t} + \mathcal{L}T = A_{HV}\frac{\partial^2 T}{\partial z^2} + A_{HH}\nabla^2 T \tag{2.5}$$

$$\frac{\partial S}{\partial t} + \mathcal{L}S = A_{HV}\frac{\partial^2 S}{\partial z^2} + A_{HH}\nabla^2 S \tag{2.6}$$

$$\rho = \rho(T, S, p) \tag{2.7}$$

where A_{HV} and A_{HH} are the vertical and horizontal eddy diffusivity coefficients for heat and salt, and

$$f = 2\Omega \sin\phi \tag{2.8}$$

is the Coriolis parameter. F^{λ} and F^{ϕ} are the eddy viscous terms,

$$F^{\lambda} = A_{MV}\frac{\partial^2 u}{\partial z^2} + A_{MH}[\nabla^2 u + \frac{(1-\tan^2\phi)u}{a^2} - \frac{2\tan\phi}{a^2\cos\phi}\frac{\partial v}{\partial\lambda}] \tag{2.9}$$

$$F^{\phi} = A_{MV}\frac{\partial^2 v}{\partial z^2} + A_{MH}[\nabla^2 v + \frac{(1-\tan^2\phi)v}{a^2} + \frac{2\tan\phi}{a^2\cos\phi}\frac{\partial u}{\partial\lambda}] \tag{2.10}$$

where A_{MV} and A_{MH} is the vertical and lateral eddy viscosity coefficients, and $\mathcal{L}$ denotes the advection operator,

$$\mathcal{L}\sigma = \frac{1}{a\cos\phi}[\frac{\partial}{\partial\lambda}(u\sigma) + \frac{\partial}{\partial\phi}(v\sigma\cos\phi)] + \frac{\partial}{\partial z}(w\sigma) \tag{2.11}$$

The horizontal Laplacian ∇^2 is given by

$$\nabla^2\sigma = \frac{1}{a^2\cos^2\phi}[\frac{\partial^2\sigma}{\partial\lambda^2} + \frac{\partial}{\partial\phi}(\cos\phi\frac{\partial\sigma}{\partial\phi})] \tag{2.12}$$

Since a large scale hydrostatic model cannot handle convection explicitly, a simple implicit convection scheme is used. In our model, when a gravitational instability is detected, the vertical eddy diffusivity takes a large value.

2.3 Boundary Conditions

Lateral walls of the basin are insulating, no-slip, impermeable boundaries,

$$u, v, T_n, S_n = 0 \tag{2.13}$$

where $(\quad)_n$ indicates a local derivative with respect to the coordinate normal to the wall.

At the bottom, the normal gradients of T and S are zero so that there are no heat and salt fluxes across the bottom,

$$\frac{\partial T}{\partial z}, \frac{\partial S}{\partial z} = 0, \qquad \text{at } z = -H(\lambda, \phi) \tag{2.14}$$

For velocities, we have

$$\rho_0 A_{MV}(\frac{\partial u}{\partial z}, \frac{\partial v}{\partial z}) = (\tau_s^\lambda, \tau_s^\phi), \qquad \text{at } z = 0 \tag{2.15}$$

$$\rho_0 A_{MV}(\frac{\partial u}{\partial z}, \frac{\partial v}{\partial z}) = (\tau_b^\lambda, \tau_b^\phi), \qquad \text{at } z = -H(\lambda, \phi) \tag{2.16}$$

$$w = 0, \qquad \text{at } z = 0 \tag{2.17}$$

$$w = -\frac{u}{a\cos\phi}\frac{\partial H}{\partial \lambda} - \frac{v}{a}\frac{\partial H}{\partial \phi}, \qquad \text{at } z = -H(\lambda, \phi) \tag{2.18}$$

Here $(\tau_s^\lambda, \tau_s^\phi)$ is the surface wind stress and $(\tau_b^\lambda, \tau_b^\phi)$ is the bottom stress,

$$(\tau_b^\lambda, \tau_b^\phi) = \rho_0 r(u_b, v_b) \tag{2.19}$$

where ρ_0 is representative density for sea water, r is bottom friction coefficient, and (u_b, v_b) the bottom velocity. Putting $w = 0$ at $z = 0$ corresponds to the rigid-lid approximation. Equation (2.18) corresponds to the kinematic boundary condition, i.e., at the ocean bottom, flow is required to parallel the slope.

The surface boundary conditions to be imposed at the sea surface on temperature and salinity are discussed in Chapter 3 and require some more modeling assumptions to be made. The air-sea interaction processes must be parameterized in running an ocean model. The implication of these modeling assumptions will be considered in much more detail in Chapter 4.

2.4 Method of Solution

The formulation of the finite difference forms of the prognostic equations requires the elimination of the surface pressure. The velocity is separated into barotropic and baroclinic components. Separate prognostic equations are solved for each.

Integrating the continuity equation (2.4) with respect to z, and combining boundary conditions (2.17) and (2.18) gives

$$\frac{1}{a\cos\phi}\frac{\partial}{\partial\lambda}\left(\int_{-H}^{0} u\,dz\right)+\frac{1}{a\cos\phi}\frac{\partial}{\partial\phi}\left(\cos\phi\int_{-H}^{0} v\,dz\right)=0. \tag{2.20}$$

The non-divergent property of the vertically integrated transport makes it possible to define a barotropic transport streamfunction, ψ, such that

$$u=\frac{1}{H}\int_{-H}^{0} u\,dz \;=\; -\frac{1}{Ha}\frac{\partial\psi}{\partial\phi} \tag{2.21}$$

$$\bar{v}=\frac{1}{H}\int_{-H}^{0} v\,dz \;=\; \frac{1}{Ha\cos\phi}\frac{\partial\psi}{\partial\lambda} \tag{2.22}$$

Integrating the hydrostatic equation from a depth $-z$ to the surface, $z=0$, gives

$$p(z)=p_s+\int_{z}^{0} g\rho\,dz' \tag{2.23}$$

The surface pressure p_s cannot be simply set equal to atmopheric pressure, but must include the pressure exerted by the rigid lid.

Taking the vertical averages of (2.1) and (2.2) yields

$$\frac{\partial u}{\partial t}-fv=-\frac{1}{\rho_0 a\cos\phi}\left[\frac{\partial p_s}{\partial\lambda}+\frac{g}{H}\int_{-H}^{0}\int_{z}^{0}\frac{\partial\rho}{\partial\lambda}\,dz'\,dz\right]+\overline{F^{\lambda}} \tag{2.24}$$

$$\frac{\partial v}{\partial t}+fu=-\frac{1}{\rho_0 a}\left[\frac{\partial p_s}{\partial\phi}+\frac{g}{H}\int_{-H}^{0}\int_{z}^{0}\frac{\partial\rho}{\partial\phi}\,dz'\,dz\right]+\overline{F^{\phi}} \tag{2.25}$$

where $\overline{(\ )} \equiv \frac{1}{H}\int_{-H}^{0}(\ )\,dz$. Using the definition of streamfunction (2.21) and (2.22) and applying the $a^2\cos\phi\,\mathrm{Curl}_z$ operator

$$\mathrm{Curl}_z(A,B) = \frac{1}{a\cos\phi}\left[\frac{\partial B}{\partial\lambda} - \frac{\partial(A\cos\phi)}{\partial\phi}\right] \tag{2.26}$$

to (2.24) and (2.25) we obtain the barotropic vorticity equation,

$$\frac{\partial}{\partial\lambda}\left(\frac{1}{H\cos\phi}\frac{\partial^2\psi}{\partial\lambda\partial t}\right) + \frac{\partial}{\partial\phi}\left(\frac{\cos\phi}{H}\frac{\partial^2\psi}{\partial\phi\partial t}\right) - \frac{\partial}{\partial\lambda}\left(\frac{f}{H}\frac{\partial\psi}{\partial\phi}\right) + \frac{\partial}{\partial\phi}\left(\frac{f}{H}\frac{\partial\psi}{\partial\lambda}\right)$$
$$= \mathrm{JEBAR} + a^2\cos\phi\,\mathrm{Curl}_z(\overline{F^\lambda},\overline{F^\phi}) \tag{2.27}$$

JEBAR is the Joint Effect of Baroclinicity And Relief (Sarkisyan and Ivanov, 1971),

$$\mathrm{JEBAR} = -\frac{\partial}{\partial\lambda}\left(\frac{g}{\rho_0 H}\int_{-H}^{0}\int_{z}^{0}\frac{\partial\rho}{\partial\phi}\,dz'\,dz\right) + \frac{\partial}{\partial\phi}\left(\frac{g}{\rho_0 H}\int_{-H}^{0}\int_{z}^{0}\frac{\partial\rho}{\partial\lambda}\,dz'\,dz\right) \tag{2.28}$$

Then ψ can be easily solved given appropriate boundary conditions. The condition of no normal flow through the lat ral walls requires that ψ be constant on the lateral boundary, Γ. We set it equal to zero,

$$\psi = 0 \qquad\qquad \text{on } \Gamma \tag{2.29}$$

To predict the baroclinic components, we first compute provisional horizontal velocities (u^*, v^*) from (2.1) and (2.2), setting $p_s = 0$,

$$\frac{\partial u^*}{\partial t} - fv = -\frac{g}{\rho_0 a\cos\phi}\int_{z}^{0}\frac{\partial\rho}{\partial\lambda}\,dz + F^\lambda \tag{2.30}$$

$$\frac{\partial v^*}{\partial t} + fu = -\frac{g}{\rho_0 a}\int_{z}^{0}\frac{\partial\rho}{\partial\phi}\,dz + F^\phi \tag{2.31}$$

The use of the true velocities in most terms in these equations is an artifact of the time integration scheme which we describe in more detail in the next section. We can obtain the true baroclinic velocity (u', v') by substracting the vertical mean of the provisional velocity, which is just the amount by which they are in error,

$$u' = u^* - \overline{u^*} \tag{2.32}$$

$$v' = v^* - \overline{v^*} \tag{2.33}$$

This is because the error in (u^*, v^*) induced by ignoring p_s is independent of depth.

Outlining the route of solution, we diagnose the density from the equation of state (2.7), the pressure from the hydrostatic equation (2.3). We update the momentum equations (2.30) and (2.31) along with (2.32) and (2.33) for the baroclinic velocity, the barotropic vorticity equation (2.27) along with (2.21) and (2.22) for the barotropic velocity, the vertical velocity can then be diagnosed from the continuity equation (2.4). Then we time integrate the tracer equations (2.5) and (2.6) for the temperature and salinity.

2.5 Discretization and Implementation

The set of equations described in the previous section are solved using finite difference methods. The Arakawa B-grid is employed for the horizontal grid arrangement. Tem-

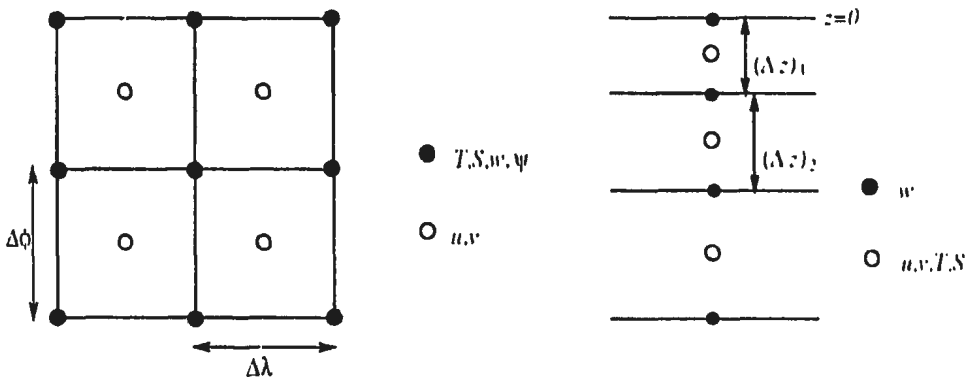

(a) Horizontal grid arrangement (b) Vertical grid arrangement

Figure 2.1: The grid arrangement of the model variables u, v, w, T, S and ψ in both the horizontal and vertical.

perature, salinity and streamfunction values are computed on one set of grid points, and horizontal velocity is computed on another set displaced one half a grid space in each direction from the temperature and salinity grids (Fig. 2.1a). Vertical velocity is diagnosed at temperature and salinity grid points at vertical levels between the primary grid levels (Fig. 2.1b). In this section, we only write down the time integration schemes. The spatial derivatives should all be replaced by their finite difference forms based on a centered-differencing scheme. The details of the finite difference equations and the proofs of their conservation properties are not given here but may be found in Bryan (1969), Semtner (1974), and Cox (1984).

Table 2.1 summarizes the parameters used in our model. In this study, our model domain is an idealized North Atlantic sized box covering the latitudes $5°N$

Table 2.1: Model Parameters

Horizontal Turbulent Viscosity	$A_{MH} = 1.0 \times 10^5 m^2/s$
Vertical Turbulent Viscosity	$A_{MV} = 1.0 \times 10^{-3} m^2/s$
Horzontal Turbulent Diffusivity	$A_{HH} = 2.0 \times 10^3 m^2/s$
Vertical Turbulent Diffusivity	$A_{HV} = 6.3 \times 10^{-5} m^2/s$
Bottom Friction Coefficient	$r = 0.001$
Equation of State	$\rho(T,S) = 3.0 + 0.77S - 0.072T(1 + 0.072T)$

Table 2.2: Vertical Grid Spacing (Unit of Depth: meters)

Level Number	Level Thickness	u, v, T, S Depth	w Depth	Level Number	Level Thickness	u, v, T, S Depth	w Depth
			0				715
1	16	23.0		8	232	831.0	
			46				947
2	58	75.0		9	292	1093.0	
			104				1239
3	73	140.5		10	368	1423.0	
			177				1607
4	92	223.0		11	463	1838.5	
			269				2070
5	116	327.0		12	584	2362.0	
			385				2654
6	146	458.0		13	673	2990.5	
			531				3327
7	184	623.0		14	673	3663.5	
							4000

- $65°N$ with 60 degree longitudinal width and a flat bottom with uniform depth of 4000 meters. The horizontal resolution is $2.4° \times 2.4°$ in longitude and latitude. There are 14 levels in the vertical direction, with resolution varying from 46 meters near the surface to 673 meters near the bottom. The depth of the primary and the vertical velocity grid levels are given in Table 2.2.

2.5.1 Time Integration Scheme

The time integration scheme used for the prognostic equations is the leap frog scheme with periodic application of an Euler forward time step to prevent the time splitting of the solution. For the baroclinic part of the velocity, from (2.30) and (2.31), we have

$$\frac{u^* - u^{(\tau-1)}}{2\Delta t} - fv^* = -\frac{g}{\rho_0 a \cos\phi}\int_z^0 \frac{\partial \rho^{(\tau)}}{\partial \lambda}\, dz + F^{u\lambda(\tau-1)} \tag{2.34}$$

$$\frac{v^* - v^{(\tau-1)}}{2\Delta t} + fu^* = -\frac{g}{\rho_0 a}\int_z^0 \frac{\partial \rho^{(\tau)}}{\partial \phi}\, dz + F^{u\phi(\tau-1)} \tag{2.35}$$

$$u'^{(\tau+1)} = u^* - \overline{u^*} \tag{2.36}$$

$$v'^{(\tau+1)} = v^* - \overline{v^*} \tag{2.37}$$

where $(\ )^{(\tau)}$ represents the variable at time level τ.

To calculate the barotropic part of the velocity, we finite-difference the barotropic

vorticity equation (2.27) as

$$\frac{\partial}{\partial\lambda}\left(\frac{1}{H\cos\phi}\frac{\partial\psi^{(\tau+1)}}{\partial\lambda}\right)+\frac{\partial}{\partial\phi}\left(\frac{\cos\phi}{H}\frac{\partial\psi^{(\tau+1)}}{\partial\phi}\right)-2\Delta t\left[\frac{\partial}{\partial\lambda}\left(\frac{f}{H}\frac{\partial\psi^{(\tau+1)}}{\partial\phi}\right)-\frac{\partial}{\partial\phi}\left(\frac{f}{H}\frac{\partial\psi^{(\tau+1)}}{\partial\lambda}\right)\right]$$
$$=\frac{\partial}{\partial\lambda}\left(\frac{1}{H\cos\phi}\frac{\partial\psi^{(\tau-1)}}{\partial\lambda}\right)+\frac{\partial}{\partial\phi}\left(\frac{\cos\phi}{H}\frac{\partial\psi^{(\tau-1)}}{\partial\phi}\right)+2\Delta t\,\mathrm{JEBAR}^{(\tau)}$$
$$+2\Delta t\,a^2\cos\phi\,\mathrm{Curl}_z(\overline{F^\lambda},\overline{F^\phi})^{(\tau-1)} \tag{2.38}$$

Noting that $\mathrm{JEBAR}^{(\tau)}$ is calculated from $\rho^{(\tau)}$ and the friction term $\mathrm{Curl}_z(\overline{F^\lambda},\overline{F^\phi})^{(\tau-1)}$ is calculated from $(u,v)^{(\tau-1)}$. Now barotropic velocity can be calculated from (2.21) and (2.22) and vertical velocity w can be diagnosed from the continuity equation. We then integate the tracer equations (2.5) and (2.6)

$$\frac{T^{(\tau+1)}-T^{(\tau-1)}}{2\Delta t}+\frac{1}{a\cos\phi}\left[\frac{\partial}{\partial\lambda}(uT)^{(\tau)}+\frac{\partial}{\partial\phi}(vT\cos\phi)^{(\tau)}\right]+\frac{\partial}{\partial z}(wT)^{(\tau)}$$
$$=A_{HV}\frac{\partial^2T^{(\tau+1)}}{\partial z^2}+\frac{A_{HH}}{a^2\cos^2\phi}\left[\frac{\partial^2T^{(\tau-1)}}{\partial\lambda^2}+\frac{\partial}{\partial\phi}\left(\cos\phi\frac{\partial T^{(\tau-1)}}{\partial\phi}\right)\right] \tag{2.39}$$
$$\frac{S^{(\tau+1)}-S^{(\tau-1)}}{2\Delta t}+\frac{1}{a\cos\phi}\left[\frac{\partial}{\partial\lambda}(uS)^{(\tau)}+\frac{\partial}{\partial\phi}(vS\cos\phi)^{(\tau)}\right]+\frac{\partial}{\partial z}(wS)^{(\tau)}$$
$$=A_{HV}\frac{\partial^2S^{(\tau+1)}}{\partial z^2}+\frac{A_{HH}}{a^2\cos^2\phi}\left[\frac{\partial^2S^{(\tau-1)}}{\partial\lambda^2}+\frac{\partial}{\partial\phi}\left(\cos\phi\frac{\partial S^{(\tau-1)}}{\partial\phi}\right)\right] \tag{2.40}$$

Here the horizontal diffusion terms are evaluated at a lag of one time step to suppress numerical instability. But the vertical diffusion terms are treated implicitly. This takes care of the parameterization of deep convection and enables a large vertical diffusion coefficient to be used when a gravitational instability is detected.

2.5.2 Restrictions and Distorted Physics

With above finite-difference scheme, there are a number of restrictions on the range of values which the grid spacing, time step, and parameters may take in order to avoid numerical instability. The first of the computational constraints which must be satisfied is the linear stability or CFL condition after Courant, Friedrich and Lewy (1928). Physically the CFL condition states that useful information must propagate less than one Δx in time Δt, i.e., $\Delta t \leq \Delta x/C$ (C is the propagating speed concerned). Since Coriolis terms in our model are treated implicitly, the restrictions of the allowed time step associated with barotropic Rossby waves and inertial waves are eliminated. The only restriction on the time step for the barotropic part comes from the mixing term. For the model parameters listed in Table 2.1, this barotropic time step is about one day. In the baroclinic part, the restriction of integration time step is associated with the first internal mode of gravity wave which is about 3 m/s. This also suggests a time step of about one day.

Compared with the atmosphere, the motion of the ocean contains a much wider range of time scales. If we use the straightforward method of integrating each of the prognostic equations, we must take short enough time steps (say, 1/2 day) to resolve internal gravity waves, but must integrate the model long enough for the thermal

fields to reach equalibrium, which may take 1000 years. This becomes prohibitively expensive for ocean climate studies. Instead, we follow Bryan (1984) and use a method based on distorted physics to speed up convergence. The distorted physics compresses the frequency band of the ocean model by slowing down gravity waves and speeding up abyssal process. The acceleration of abyssal process is accomplished by decreasing the local heat capacity without altering the transport and mixing of heat. This means that changes within one time step in deep water are equivalent of the changes that happen within many time steps under non-distorted physics, but the distorted system has the same equilibrium solution as the original system. Acceleration is used only in the spin-up experiment to be described. For the interdecadal variability studies, the acceleration technique is not used.

Chapter 3

OGCM Coupled with Zero-heat Capacity Atmosphere

3.1 Spin up

3.1.1 Restoring Boundary Condition

Considering the surface heat balance for an ocean in equilibrium with an atmosphere which is constant in time, Haney (1971) wrote the heat flux into the ocean as

$$Q = \gamma(T^* - T_s) \tag{3.1}$$

where T_o is the temperature at ocean surface, T^* is the so-called "effective atmosphere temperature", and the coupling constant γ represents the sensitivity of the latent, sensible and longwave fluxes to changes in T_o. A typical value of γ is about 45 $Wm^{-2}K^{-1}$ (Haney 1971), which is associated with a time scale

$$\tau = \frac{c_p \rho_0 \Delta z}{\gamma},$$

here c_p, ρ_0, and Δz are the specific heat of sea water, density, and mixed-layer thickness, respectively. If we take Δz as the thickness of the top model level (46 meters), the time scale is about 50 days.

Compared with simply prescribing a constant heat flux at the ocean surface, this linear Haney-type restoring boundary condition allows feedback between ocean temperature and surface heat flux. More often, a matter-of-fact approach is used,

$$Q = \gamma(SST - T_o) \tag{3.2}$$

where SST is observed sea surface temperature. The ocean dynamics (i.e. advection and convection process) make T_o deviate from the restoring temperature SST but never allows it to go too far provided that the restoring time scale is small compared to the dynamical time scale. This restoring boundary condition is welcomed by ocean modellers because it guarantees realistic ocean surface temperatures, though it lacks physical justification like Haney's (but for climate change studies, Haney's is not

suitable because he assumed a constant atmosphere). Equation (3.2) is a form of *data assimilation*. Here γ is a nudging parameter (Tziperman and Bryan, 1993). Its value depends on how close we want the surface temperature to approach the observed SST since we know there are uncertainties in observed data and in the model. If the data and the model are perfect, then $1/\gamma$ may equal zero. This boundary condition then degenerates into a fixed-surface-temperature condition.

A similar boundary condition is often applied to salinity

$$Q_s = \gamma(SSS - S_o) \tag{3.3}$$

where SSS is observed sea surface salinity and S_o is the salinity in the top model level. Note that a surface boundary condition for salinity equivalent to (3.1) can not be justified physically since fresh water flux and surface salinity do not have a similar feedback. Rather (3.3) can be justified only on the basis of *data assimilation*.

When a restoring condition like (3.2) or (3.3) is used to drive an ocean model, the effect is to make the model value to approach the data. If the model value is colder (or fresher) than the restoring data, the heat (or salt) is put into the ocean, otherwise heat (or salt) is taken out. The rate of heat (or salt) input is proportional to the difference between the model value and the restoring data.

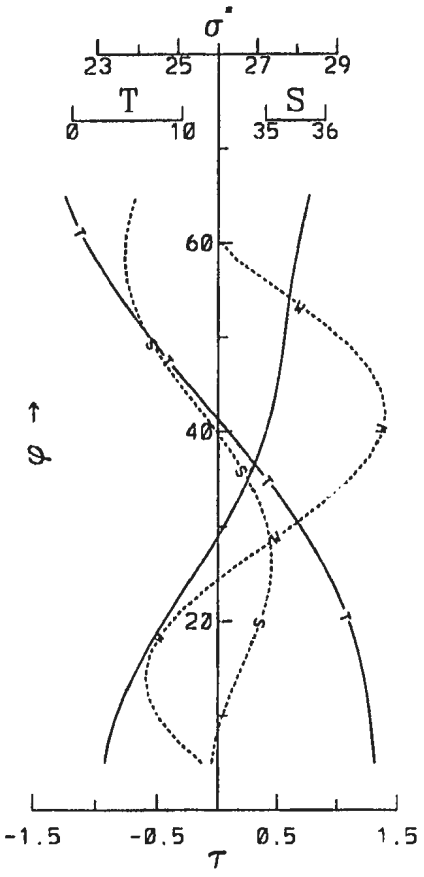

Figure 3.1: The latitudinal (°N) distributions of the surface wind stress (label W), atmospheric "equivalent" temperature (T), and salinity (S). The corresponding density σ^* is shown by the unlabeled solid curve. (From Fig.1 in ZGL 1993)

3.1.2 Spin-up with restoring boundary conditions

First, we spin up the ocean from rest. The surface wind stress forcing is zonally uniform. The eastward component is shown in Fig. 3.1, the northward component is zero. Restoring boundary conditions are applied to temperature and salinity. The "equivalent atmospheric" values used are shown in Fig. 3.1 and are zonally uniform. Values of temperature and salinity in the top level of the model are relaxed to these

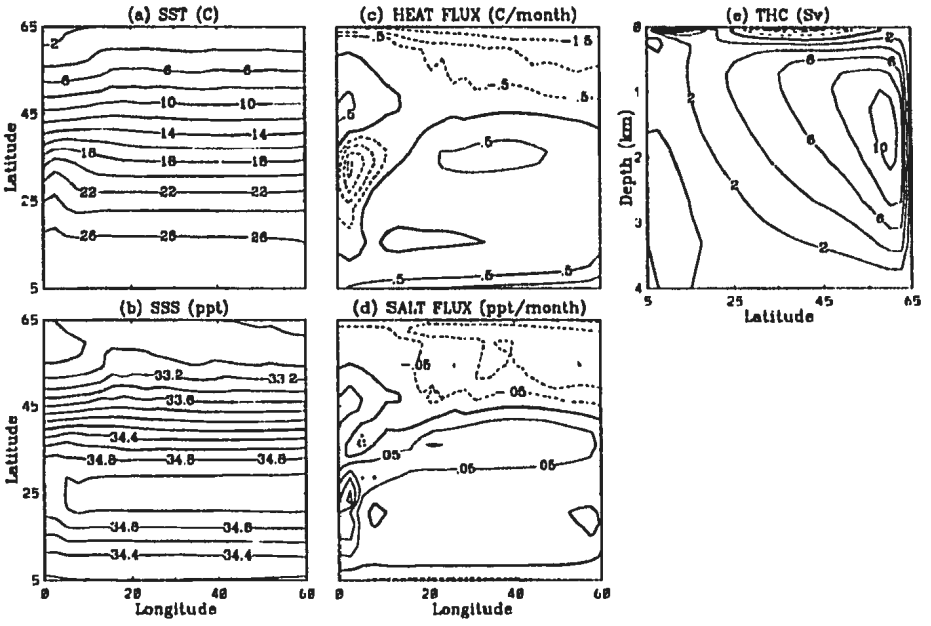

Figure 3.2: Model Variables at the End of Spin-up

values on a time scale of 30 days. The ocean is at rest at the beginning with uniform values for temperature (4°C) and salinity (35 ppt). The model runs until a steady state is reached with no trends in basin mean quantities. It takes about 1500 years in our experiment. Some model variables at the final equilibrium state of this spin-up experiment are shown in Fig. 3.2. The meridional overturning streamfunction is dominated by an overturning cell with sinking near the northern boundary and smaller cells near the surface that are due to the wind-driven Ekman pumping. The surface heat and salt fluxes shown in Fig. 3.2c,d are diagnosed from the final state of the spin-up experiment and are the average of $Q = \gamma(SST - T_*)$ and $Q_s = \gamma(SSS - S_*)$

(cf. equations (3.2) and (3.3)) over the last three years of integration. Fig. 3.2 is very similar to Fig. 2 and Fig. 3 in ZGL. Note that, following the general practice (but see Huang, 1993), we work with an equivalent surface salt flux, Q_s, rather than freshwater flux, Q_f. The two are related by

$$Q_s = \frac{(E-P)}{\Delta z}\bar{S}$$

where $\bar{S}$ is a constant reference salinity.

3.2 Coupling to Schopf's Model

3.2.1 Schopf's Model

The assumption of a Haney-type restoring boundary condition is that the atmosphere is time invariant, i.e., has *infinite heat capacity*. The effective atmospheric temperature T^* remains constant despite changes in surface heat flux from the ocean. Bretherton (1982) has noted that this is only true when the thermal anomaly has a small horizontal scale (compared to the basin scale), especially in regions of strong atmospheric transport of heat where winds rapidly disperse the additional heat entering the atmosphere from the ocean. This process has a time scale of tens of days, as under a Haney-type restoring boundary condition. On the other hand, for large

scale SST anomalies, radiative relaxation from the atmosphere plays a major role. Schopf (1983) has pointed out that the air-sea temperature difference in the tropics is rarely more than 1°C. There is also a close connection between SST and surface air temperature in the North Atlantic (Deser and Blackmon, 1993). Schopf suggested that a better approach to model heat exchange between the atmosphere and the ocean is to use a simple atmospheric heat budget and assume the atmosphere has zero heat capacity.

Following Schopf, we use a very simple model which describes the thermal coupling between the atmosphere and the ocean:

$$C_a \frac{\partial T_a}{\partial t} = -K(T_a - T_o) - K_r' T_a + Q_a \tag{3.4}$$

$$C_o \frac{\partial T_o}{\partial t} = K(T_a - T_o) + Q_o \tag{3.5}$$

Here T_o is the sea surface temperature, and T_a the representative atmospheric temperature; C_a and C_o are the heat capacities of the atmosphere and the ocean mixed layer (the top level of the ocean model); K_r' is the constant for a linearized Stefan's Law for atmospheric longwave radiation; and Q_a and Q_o stand for the atmospheric and oceanic heat sources due to advection, eddy diffusion and solar radiation. Since C_a/C_o is only about 0.045, Schopf set $C_a = 0$, i.e., the heat capacity of the atmosphere

is zero as far as local changes in T_a are concerned. Now equation (3.3) becomes

$$0 = -K(T_a - T_o) - K_r'(T_a - T_r) \tag{3.6}$$

where

$$T_r = Q_a / K_r' \tag{3.7}$$

Solving (3.6) for T_a,

$$T_a = \frac{KT_o + K_r'T_r}{K + K_r'} \tag{3.8}$$

Substituting (3.8) into (3.5), we get

$$C_o \frac{\partial T_o}{\partial t} = K_r(T_r - T_o) + Q_o \tag{3.9}$$

where

$$K_r = \frac{K K_r'}{K + K_r'} \tag{3.10}$$

Typically, $K = 45 W m^{-2} K^{-1}$ (Haney 1971) and $K_r' = 2.4 W m^{-2} K^{-1}$ (Dickinson 1981), therefore $K_r = 2.3 W m^{-2} K^{-1}$. This is 20 times smaller than K. One can use (3.9) as a thermal boundary condition for ocean-only models, in which sea surface temperature T_o is restored to a time independent T_r with a time scale of close to 600 days, instead of (3.3), which restores T_o to T_a with a time scale of about 30 days. This is the zero-heat-capacity model adopted by Schopf (1983) and will subsequently be referred to as Schopf's model. It is appropriate when the sea surface temperature

anomalies in the model have basin scale. Then, heat cannot be advected by winds and reabsorbed by the ocean, and the atmosphere must warm up until longwave radiation to space balances the increased heat flux from the ocean. Since the longwave radiation obeys a linearized Stefan's Law, its dependency on temperature is weak compared to the strong ocean-atmosphere coupling. Therefore the atmosphere will warm almost as much as the underlying ocean. This can be illustrated by (3.8). Since $K'_l \ll K$, (3.8) becomes $T_a \simeq T_o + \frac{K'_l}{K} T_r$, i.e., the representative atmospheric temperature is never far removed from the underlying SST.

Since the changes in SST associated with interdecadal variability of the thermohaline circulation have basin scale, we follow Zhang, Greatbatch and Lin (1993) and use Schopf's model to provide the thermal boundary condition at the surface of our ocean model.

3.2.2 The Control Run

Following ZGL, we employ equation (3.9), with T_r fixed in time, to provide a restoring surface boundary condition on temperature, and the salt flux shown in Fig. 3.2d to provide a flux condition on salinity. We wish to initialize with the final state of the spin-up experiment. Letting T_1 be the surface temperature in this state, we can

diagnose T_r through the following relation

$$\mathrm{FLUX} = K_r(T_r - T_1), \tag{3.11}$$

where FLUX is the heat flux from the atmosphere to the ocean at the end of the spin up experiment and is shown in Fig. 3.2c. We choose K_r so that it corresponds to a restoring time of 400 days. In order to reproduce ZGL, a negative salinity anomaly of 0.04 ppt is also added to the top three levels north of $50°N$.

The interdecadal oscillations in ZGL are reproduced. A fresh water pool in high latitudes appears and is advected toward the eastern boundary where it sinks, only to reappear again in the interior of the high latitude ocean before being advected once more to the eastern boundary. This event undergoes three cycles in the first 66 years after the switch (see Fig. 3.3). After 70 years, the model settles down and remains in a state essentially the same as that of the initial condition. It is worth mentioning that from Fig. 3.3 we can see the intensity of the thermohaline circulation also oscillates corresponding to changes in sea surface temperature and salinity. The thermohaline circulation does not, however, collapse at any time during the experiment.

ZGL carried out another experiment which uses mixed boundary conditions, i.e. a restoring condition on temperature and a flux condition on salinity. The restoring boundary condition on temperature was the same as in the spin up. The salt flux was

the same as diagnosed as the end of the spin up. Upon a switch from the final state of the spinup to these boundary conditions, a polar halocline catastrophe (PHC) occurs and the thermohaline circulation collapses. Indeed, a switch to mixed boundary conditions can lead to many dramatic events as noted by previous authors, ranging from the PHC (Bryan 1986a, 1986b), to "flushes" (Marotzke 1989; Weaver and Sarachik 1991a,b). Bryan (1986a) describes the PHC as a strengthening and spreading of the polar halocline. He noted that as the halocline develops, deep convection is interrupted and the meridional overturning circulation weakens dramatically while at the same time becoming increasingly confined to the upper layers of the ocean. In this way, the dense bottom water is no longer ventilated from the surface and is gradually warmed diffusively. Eventually, the bottom water becomes sufficiently warm that it is less dense than the fresh water overlying it, and a violent overturning event, a "flush", as described by Marotzke (1989), will occur. ZGL showed that for a PHC event to occur the heat loss from the ocean to the atmosphere must reduce at high latitudes. The use of mixed boundary conditions assumes that the atmospheric state is fixed and does not respond to changes in heat flux from the ocean. If the atmosphere were allowed to adjust to changes in this heat flux, then a reduction in heat loss, and hence a PHC, would be less likely to happen. This was demonstrated by coupling the ocean model to Schopf's zero-heat-capacity atmospheric model.

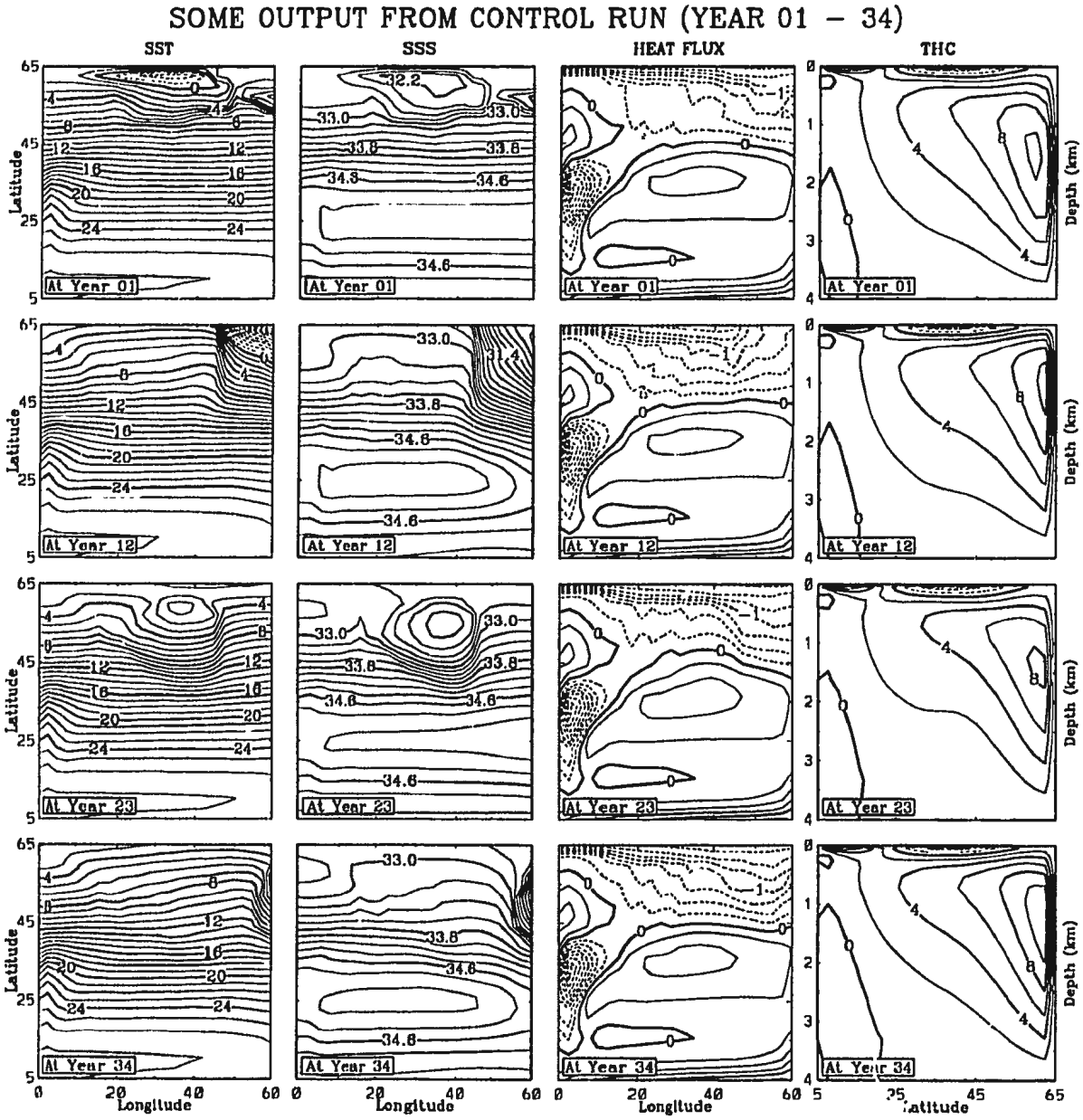

Figure 3.3: Model variables undergo three cycles with a period of about 22 years after switching to a "slowly" restoring boundary condition on emperature implied by Schopf's zero-heat-capacity atmosphere and a flux condition on salinity which is shown in Fig. 3.2d.

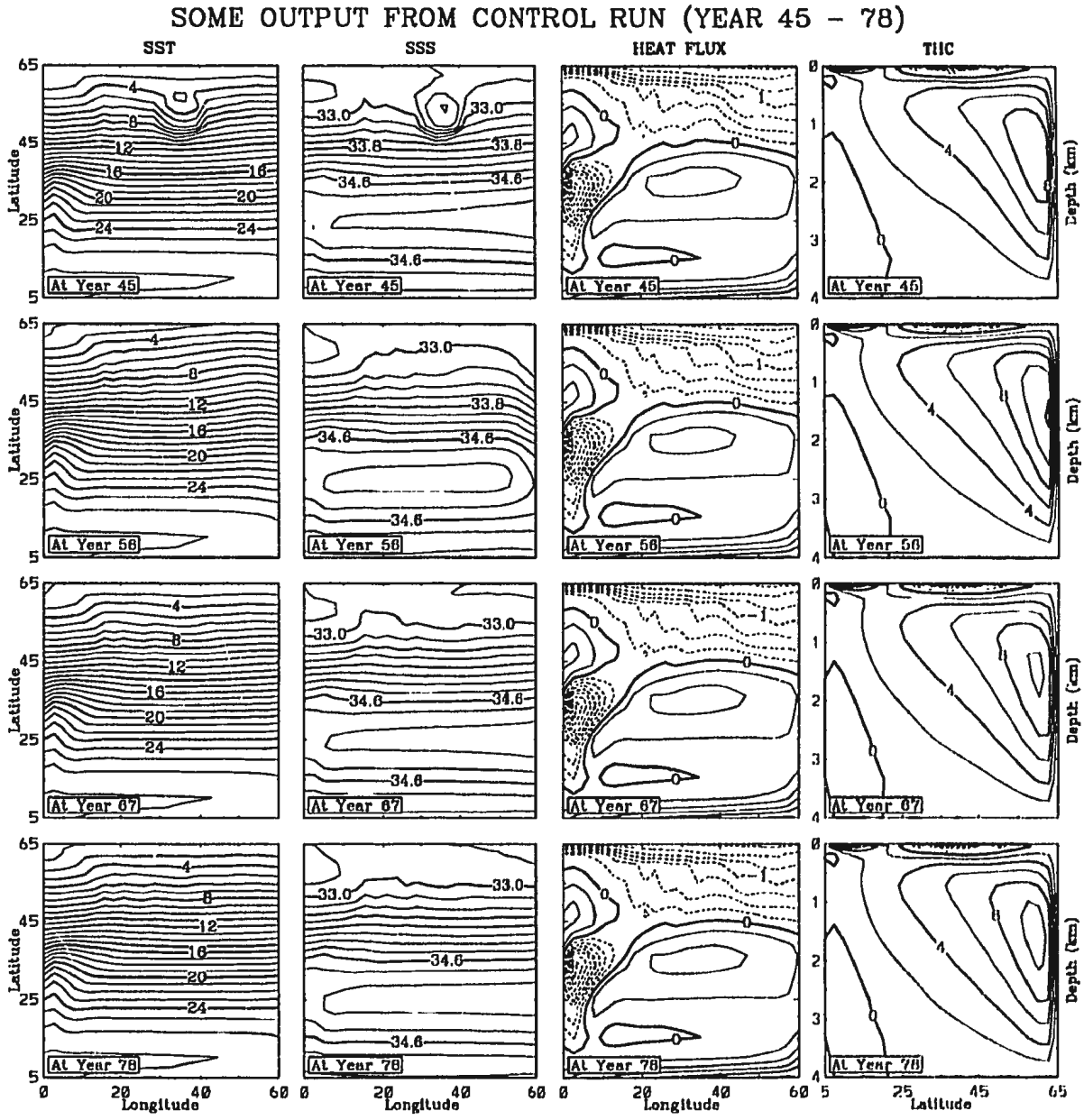

Figure 3.3: Continued.

Chapter 4

Simulation of Interdecadal Variations

4.1 Introduction

Compared to sea surface temperature and salinity data, the surface heat and freshwater flux data are poorly known. Ocean general circulation models can be used to estimate air-sea fluxes if we are given the surface distributions of the observed temperature and salinity. The problem is that the fluxes calculated in this way often tend to have noisy spatial distributions and are sometimes inconsistent with other flux estimates such as climatological fluxes obtained from meteorological ship data or

atmospheric models. Tziperman and Bryan (1993) tried to make the fluxes calculated by OGCMs consistent with the other flux estimates by combining surface restoring boundary conditions such as (3.2) and (3.3) with climatological flux data. Through an optimization approach, the surface property and climatological flux estimates are "revised" so as to keep them as consistent as possible with each other and the model dynamics within the *a priori* error bars (i.e. the "revisions" are kept as far as possible within the error bars of the observation data).

Once a set of consistent, decadally-varying surface data (SST, SSS, heat-flux and salt-flux) and an initial field are available, can we use them to deduce the interdecadal variations of the thermohaline circulation? If we can, since the surface property data and flux data are not independent of each other, what kind of surface data can we use to drive the ocean model? Because of the uncertainty and unavailability of the surface flux data (e.g., poor estimation of precipitation over the ocean and river runoffs, Clarke, 1992), can we use surface temperature and salinity data in place of the flux data? In this study, we want to develop some answers to the above questions in an idealized domain before attempting realistic simulations using real data in future work.

In the last chapter, we coupled the ocean model to Schopf's zero-heat-capacity atmosphere and observed interdecadal-type oscillations in ocean temperature, salinity

and thermohaline circulation. The interdecadally-varying 4-D ocean variables output from the control run form our data set. We sample the data only once each year for 100 years in order to represent the interdecadal variations in the data and meanwhile to save computer disk space. Data are instant values obtained directly from the control run, with no averaging applied.

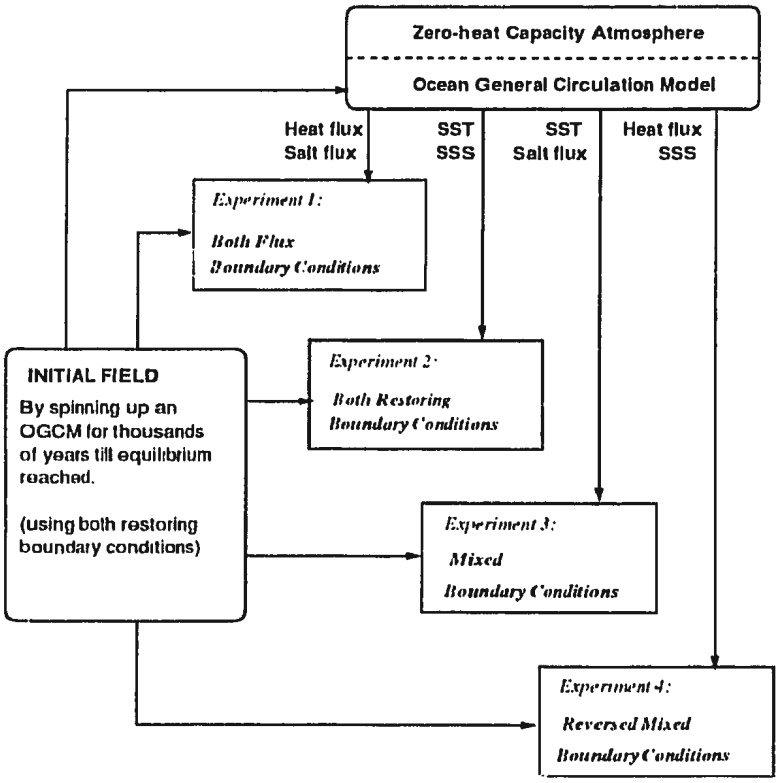

Figure 4.1: A diagram that shows how the experiments are arranged.

In this chapter we set up four experiments (see Fig. 4.1) to test the behavior of the ocean model under different surface boundary conditions on temperature and

salinity. The wind forcing is identical for all experiments in this study and is shown in Fig. 3.1. All the four experiments are initialized with the final equilibrium state of the spin-up shown in Fig. 3.2.

We use the maximum values of meridional overturning streamfunction to represent the intensity of the thermohaline circulation. We search for this maximum in the area below 800 metres to avoid including the Ekman cell in the shallow water.

4.2 Model Results

Experiment 1: Both-flux Boundary Conditions

In this experiment, we do not use sea surface temperature and salinity data. The time-dependent heat flux data (shown in Fig. 3.3, the third column) and salt flux data (Fig. 3.2d) from the control run are imposed on the top level of the ocean model each year. Here the heat flux forcing is kept constant for a year (the salt flux data is actually time-invariant anyway). Results are shown in Fig. 4.2. We can see that the thermohaline circulation, temperature and salinity field in the model results are almost identical with that in the data from the control run. Their agreement is natural because had we sampled the data every time step, we would have simply re-run the control run. This experiment shows both-flux boundary conditions can withstand

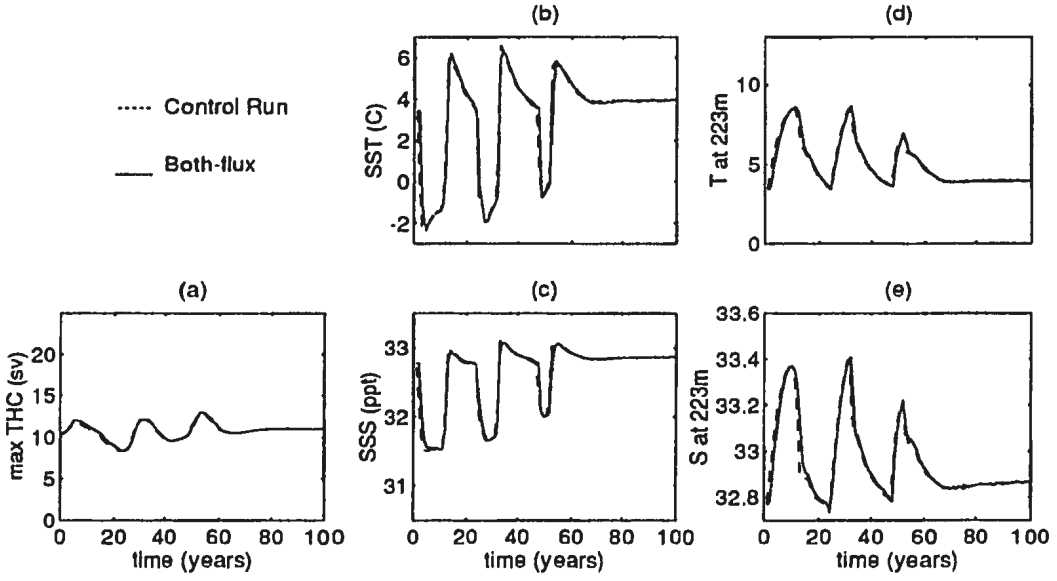

Figure 4.2: Experiment 1: Both-flux boundary conditions. (a) Maximum thermohaline circulation; (b) surface temperature; (c) surface salinity; (d) temperature at 223 m; and (e) salinity at 223 m. All but (a) are for a point at 43.2°E, 57.8°N.

some noise in the flux data. The heat flux forcing is really a "stair" function since the data are only sampled once each year and no interpolation is applied. Another source of noise is that the data are instantaneous values output from the control run, not an average over a period of time.

Greatbatch and Zhang (1993) have recently found that there is an interdecadal oscillation under a *constant*, zonally uniform heat flux forcing. This raises a question as to whether or not flux data contain full information on interdecadal variations in the coupled ocean-atmosphere system.

Experiment 2: Both-restoring Boundary Conditions

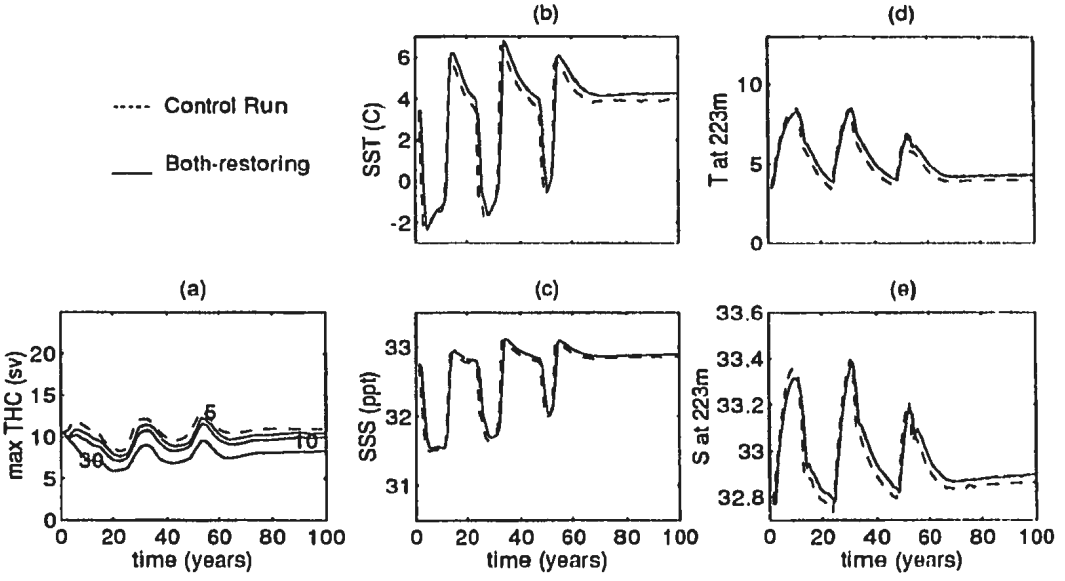

Figure 4.3: Experiment 2: Both-restoring Boundary Conditions. (a) Maximum thermohaline circulation (for restoring times 30, 10 and 5 days); (b) surface temperature; (c) surface salinity; (d) temperature at 223 m; and (e) salinity at 223 m. all but (a) are for a point at 43.2°E, 57.8°N and the restoring time is 10 days.

In this experiment, both temperature and salinity of the top model level are forced to relax to the time-dependent SST and SSS data from the control run with a time constant of 5, 10 and 30 days. Fig. 4.3a shows that the shorter the restoring time scale, the closer the thermohaline circulation approaches the control-run data. This is also true of the temperature and salinity fields, including those at depth. The second columns of Figs. 4.4–4.8 give plan views of the model variables every 11 years and should be compared with the first columns which show the control-run fields.

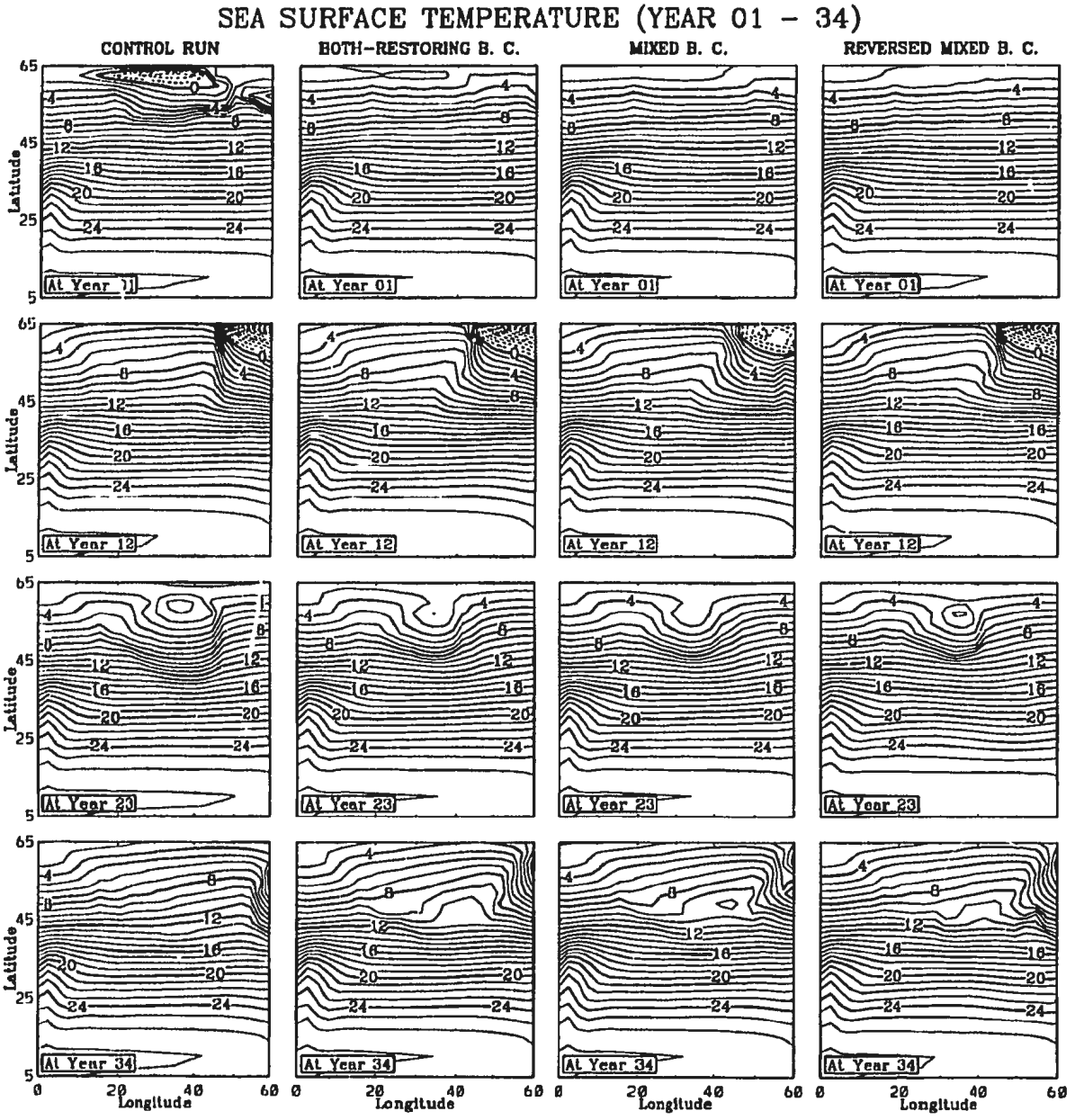

Figure 4.4: Plan views of SST in the control run, the both-restoring boundary condition case, the mixed boundary condition case, and the reversed mixed boundary condition case (from left to right). The restoring time is 10 days.

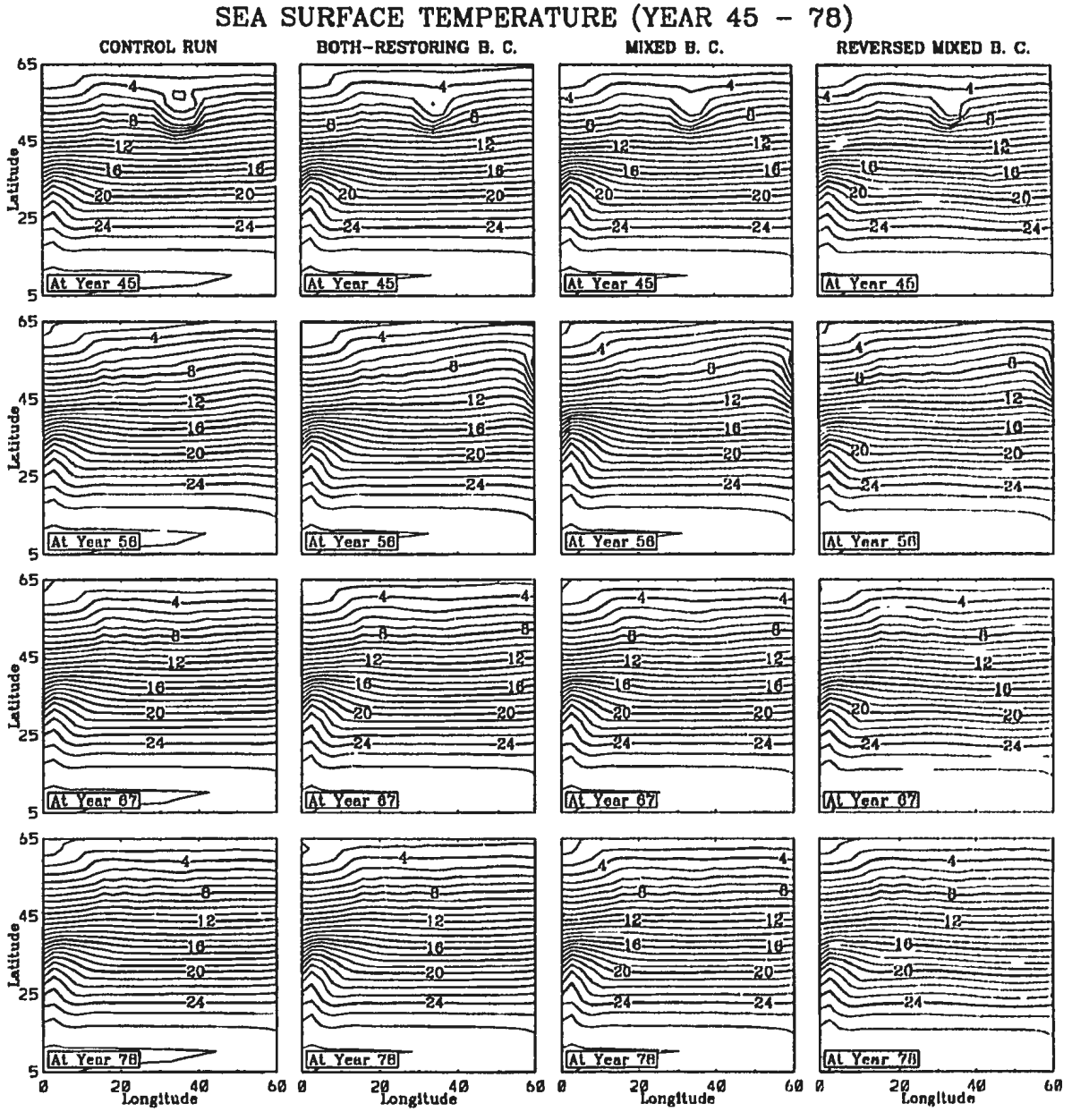

Figure 4.4: Continued.

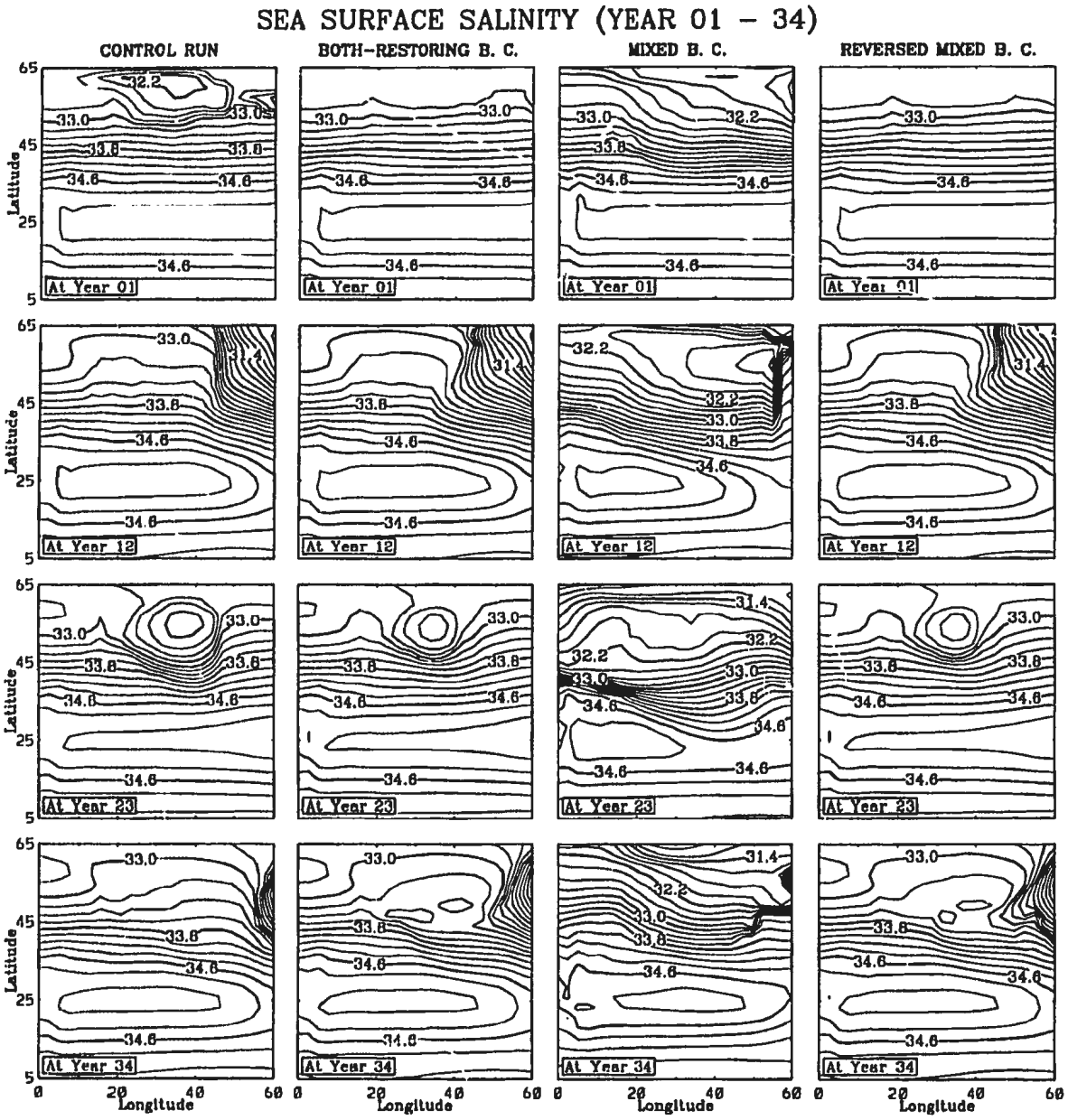

Figure 4.5: Plan views of SSS in the control run, the both-restoring boundary condition case, the mixed boundary condition case, and the reversed mixed boundary condition case (from left to right). The restoring time is 10 days.

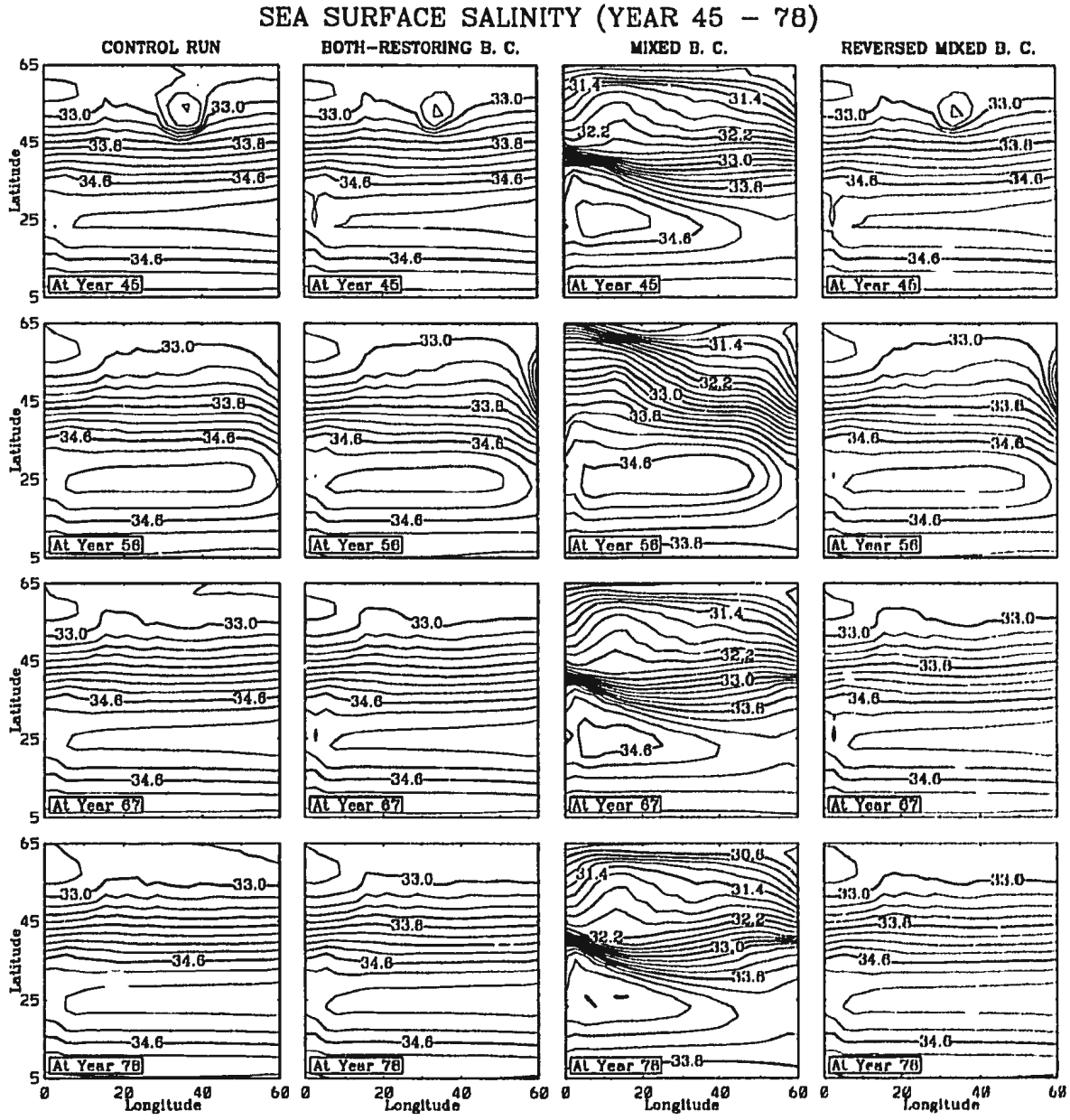

Figure 4.5: Continued.

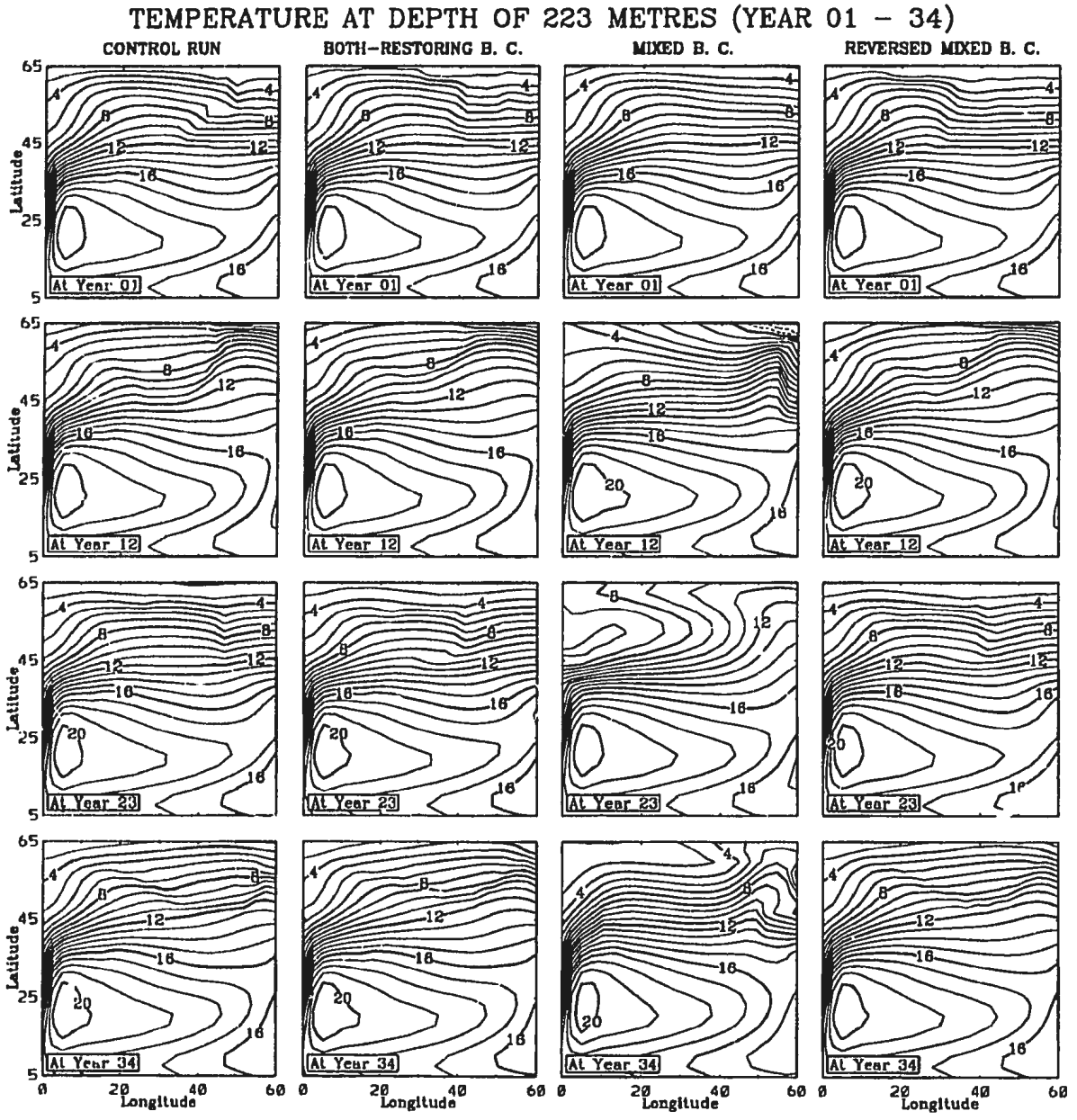

Figure 4.6: Plan views of T at 223 m in the control run, the both-restoring boundary condition case, the mixed boundary condition case, and the reversed mixed boundary condition case (from left to right). The restoring time is 10 days.

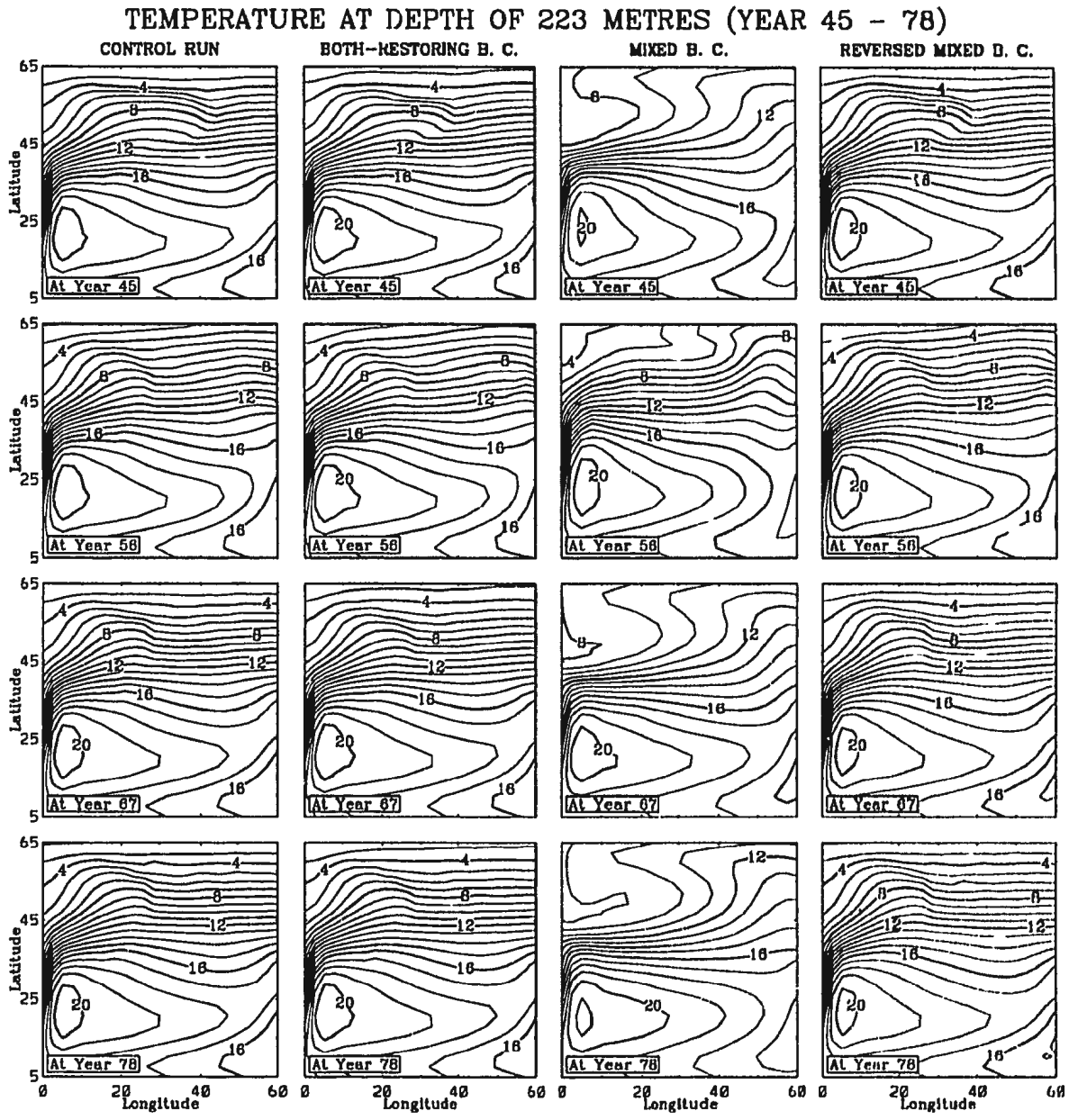

Figure 4.6: Continued.

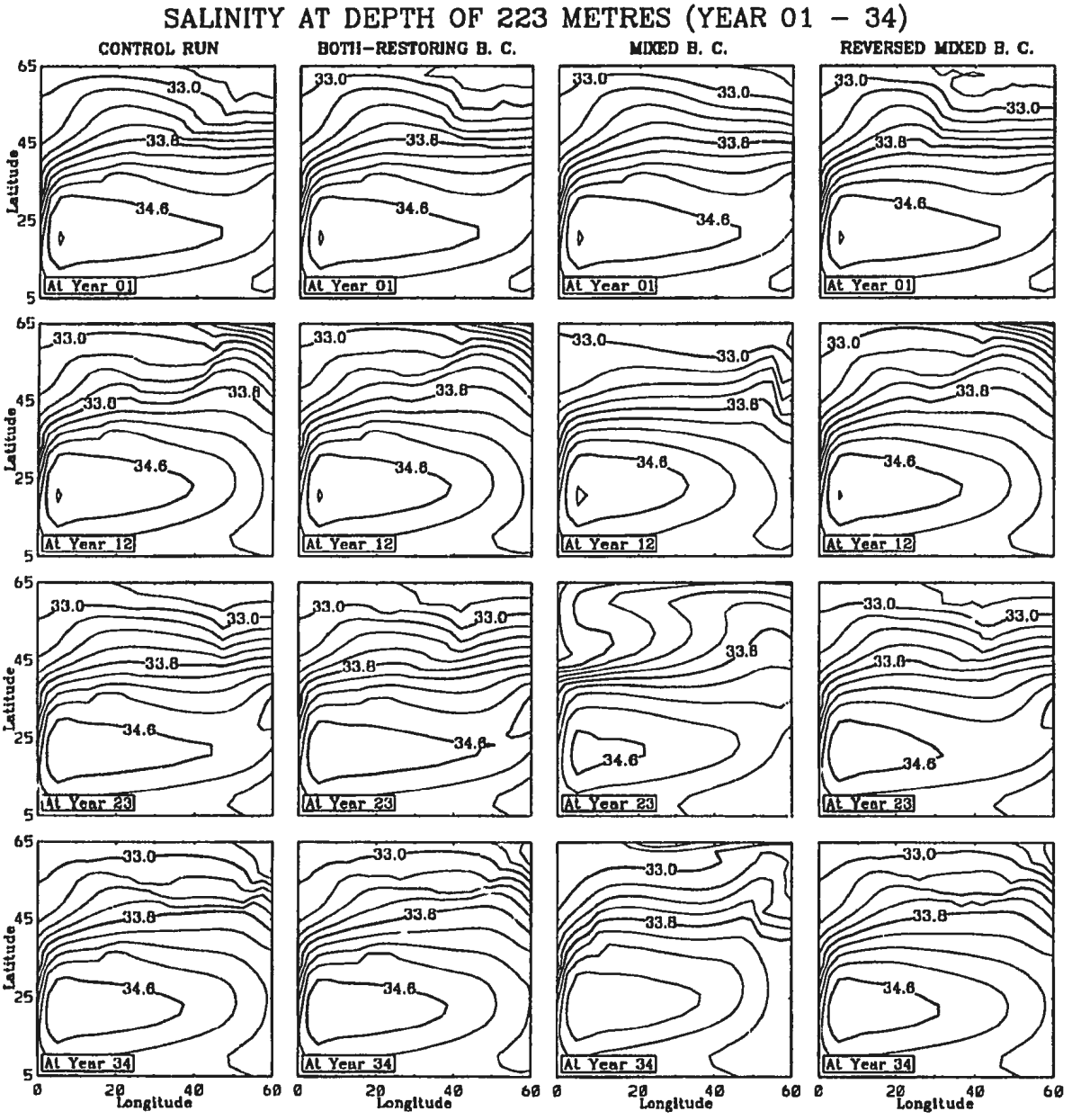

Figure 4.7: Plan views of S at 223 m in the control run, the both-restoring boundary condition case, the mixed boundary condition case, and the reversed mixed boundary condition case (from left to right). The restoring time is 10 days.

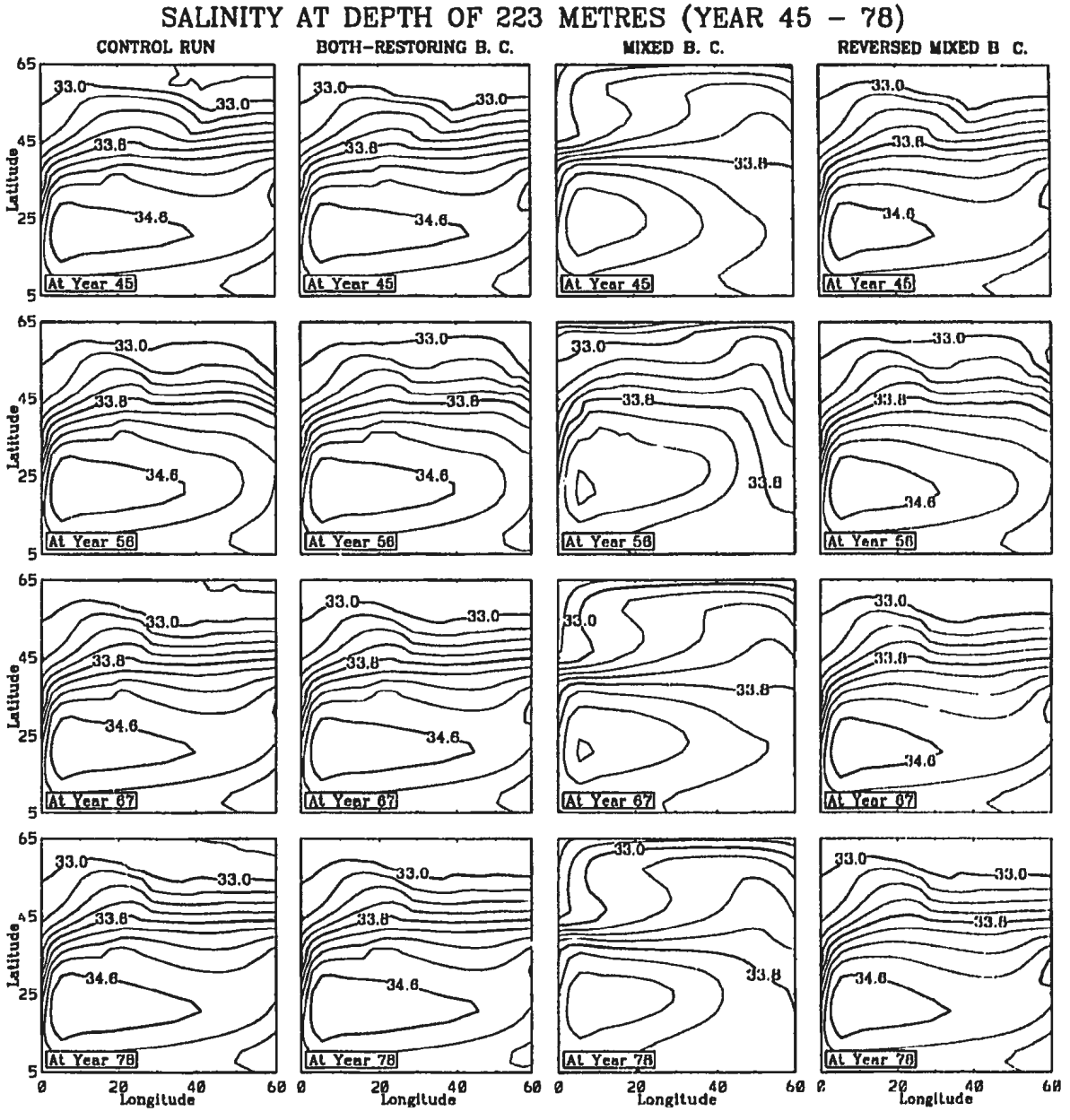

Figure 4.7: Continued.

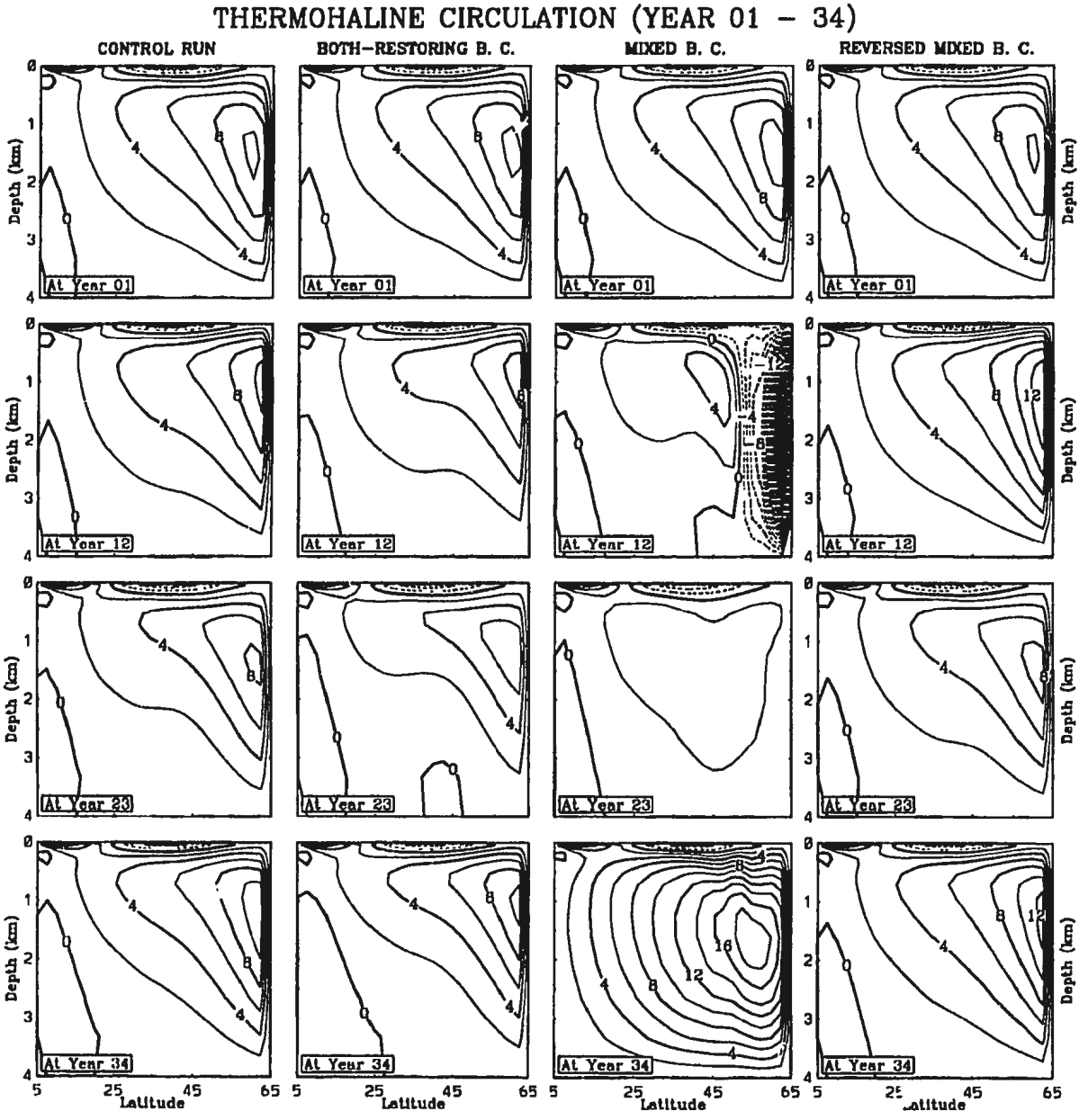

Figure 4.8: Thermohaline Circulation in the control run, the both-restoring boundary condition case, the mixed boundary condition case, and the reversed mixed boundary condition case (from left to right). The restoring time is 10 days.

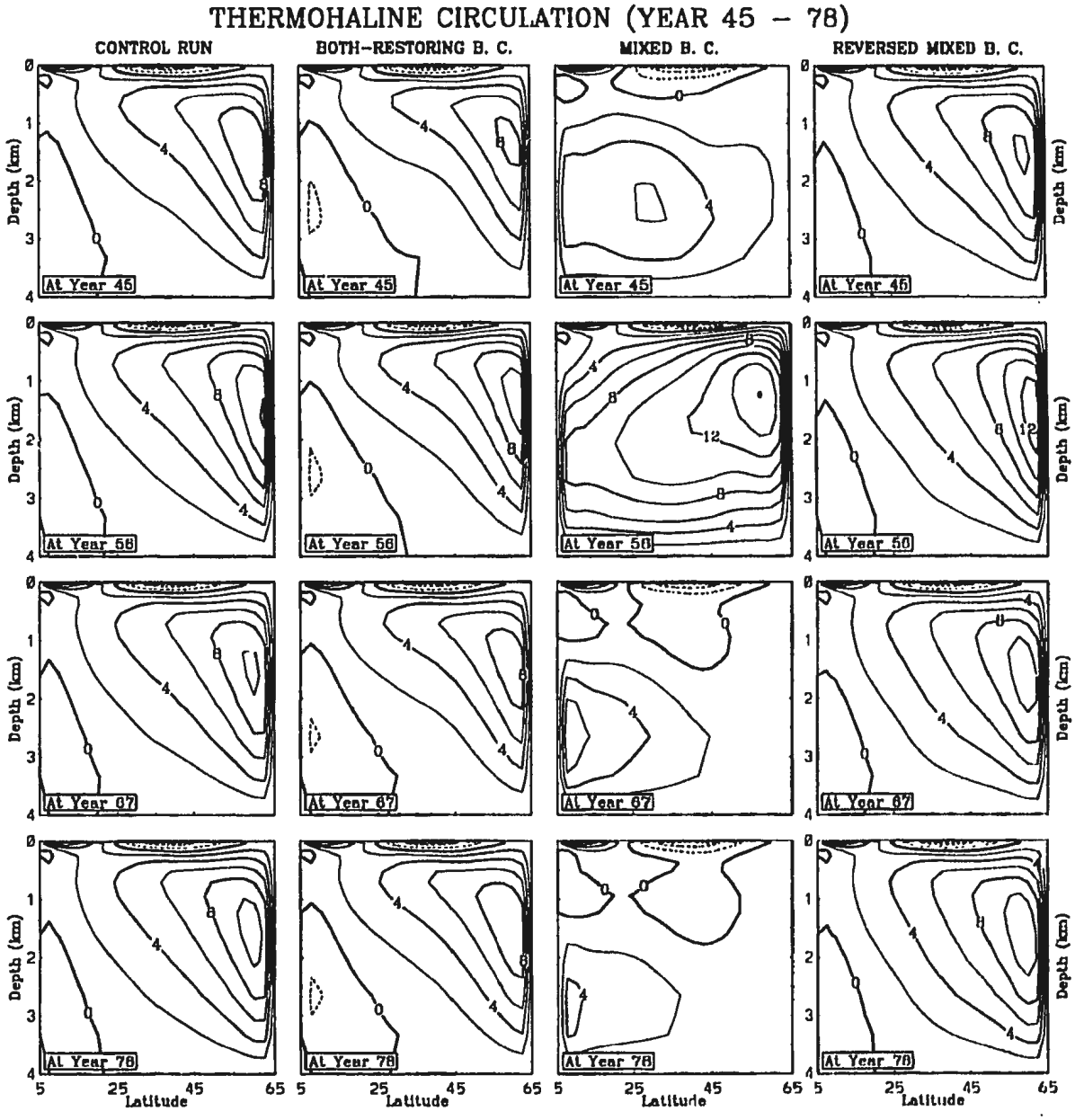

Figure 4.8: Continued.

Experiment 3: Mixed Boundary Conditions

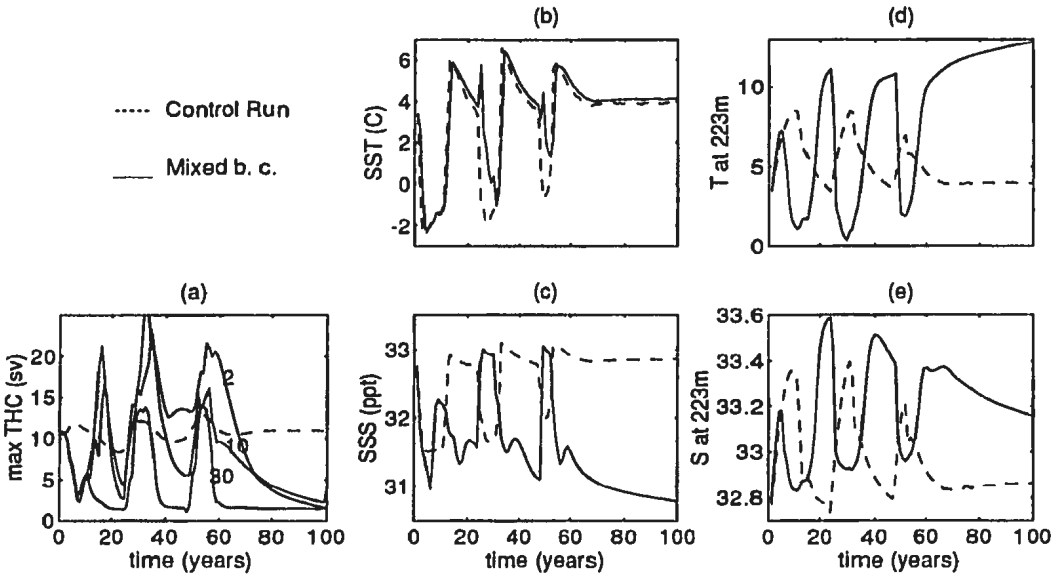

Figure 4.9: Experiment 3: Mixed Boundary Conditions. (a) Maximum thermohaline circulation (for restoring times 30, 10 and 2 days); (b) surface temperature; (c) surface salinity; (d) temperature at 223 m; and (e) salinity at 223 m. All but (a) are for a point at 43.2°E, 57.8°N and the restoring time is 10 days.

In this experiment, the time-dependent SST and salt-flux data are used to drive the model, i.e., we use a restoring boundary condition on temperature and a flux condition on salinity. After Bryan (1986a,b), it is referred to as mixed boundary conditions. Surface temperature has been relaxed to SST data on time scales of 2, 10 and 30 days. Fig. 4.9a shows the failure in this case to get the right thermohaline circulation regardless of the restoring time scale. The thermohaline circulation oscillates between a collapsed state (PHC) and a violent overturning ("flush") state (Fig. 4.8,

the third column). Surface salinity goes too far from the data (compare the 3rd column with the 1st in Fig. 4.5) and is out of phase (Fig. 4.9c) with the control run. Although a restoring boundary condition is used on surface temperature, the surface temperature is not as close to the data as that in other experiments (Fig. 4.9b). Sub-surface temperature and salinity are very different from the control-run data (Fig. 4.9d,e and Figs. 4.6 – 4.7).

Experiment 4: Reversed Mixed Boundary Conditions

Time-dependent heat-flux and sea surface salinity (SSS) data from the control run are used in this experiment, i.e., a flux condition is applied to the surface temperature and a restoring condition to the surface salinity. To distinguish it from mixed boundary conditions, we label it as "reversed mixed" boundary conditions. Fig. 4.10a shows that the thermohaline circulation is closer to the data as the restoring time is shorter. For a restoring time of 10 days, it is shown that all the thermohaline circulation, temperature and salinity are well reproduced. Forming a sharp contrast to the mixed boundary condition case, surface temperature in this case is very realistic although a flux condition is used on temperature (Fig. 4.4). The 4th columns of Figs. 4.4-4.8 give the plan views of the model variables in this experiment. Comparing with the 1st columns shows that the variables are in good agreement with the control run.

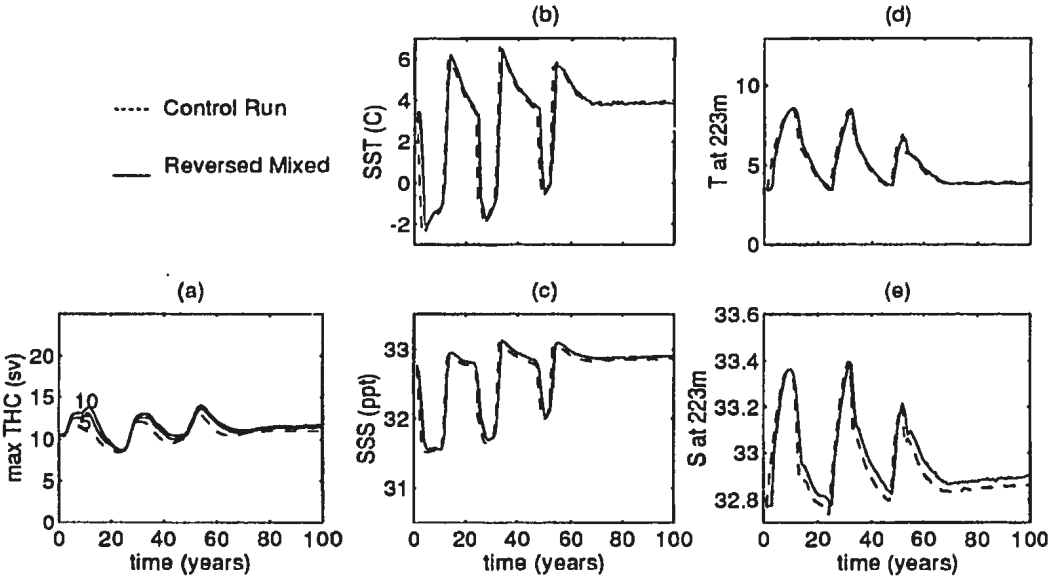

Figure 4.10: Experiment 4: Reversed Mixed Boundary Conditions. (a) Maximum thermohaline circulation (for restoring times 10 and 5 days); (b) surface temperature; (c) surface salinity; (d) temperature at 223 m; and (e) salinity at 223 m. All but (a) are for a point at 43.2°E, 57.8°N and the restoring time is 10 days.

4.3 Discussion

As mentioned in Chapter 1, the thermohaline circulation is maintained by heat loss through deep convection at high latitudes. Changes in the intensity of the thermohaline circulation will influence the temperature distribution through poleward heat transport. At high latitudes, there is always a positive freshwater flux at the sea surface. Usually this is mixed down by deep convection due to the surface heat loss. If for some reason the surface heat loss is reduced, deep convection is limited to shallower layers and a freshwater cap will develop and break the thermohaline circulation. This happens under mixed boundary conditions since neither the surface heat flux nor the surface salinity are directly controlled. This is the fundamental problem with mixed boundary conditions.

In mixed and reversed-mixed boundary condition experiments, only one surface property is controlled by a restoring condition. Although a restoring boundary condition can guarantee a correct surface value, the variable to which a flux condition is applied is not automatically guaranteed to be correct. Neither are the sub-surface values of any variables. Analyzing the behavior of the uncontrolled variables is the key to understanding the behavior under each set of boundary conditions.

In order to see clearly what happens under mixed boundary conditions, Fig. 4.9

is re-drawn in Fig. 4.11 and the implied surface heat flux is calculated from (3.2) and added into Fig. 4.11. The most obvious features in Fig. 4.11 are that high surface salinity peaks are corresponding to enormous surface heat losses and followed by an enhancement of the thermohaline circulation, and surface freshening is corresponding to surface heat-loss reduction and followed by a collapse of the thermohaline circulation (compare (d), (c) and (a) in Fig. 4.11). These features are not in agreement with the control run. Indeed the phase of surface salinity is contrary to that in the control run.

The reason why the mixed boundary condition case behaves as it does in Fig. 4.11 is that it allows a positive feedback between the development of a freshwater cap and heat-loss reduction at high latitudes. The rate of surface heat-loss changes all the time when a restoring condition is applied to surface temperature using the time-varying SST data from the control run. Neither surface heat flux nor surface salinity is a controlled variable under mixed boundary conditions. When the surface temperature in the data is going up, surface heat-loss reduction occurs (Fig. 4.11d) and the deep convection process is weakened. The reduced vertical convection then mixes the freshwater flux over a shallower water column, resulting in a development of a freshwater cap. This stabilizes the water column and eventually switches off the overturning thermohaline circulation. It is also the reason why the surface salinity

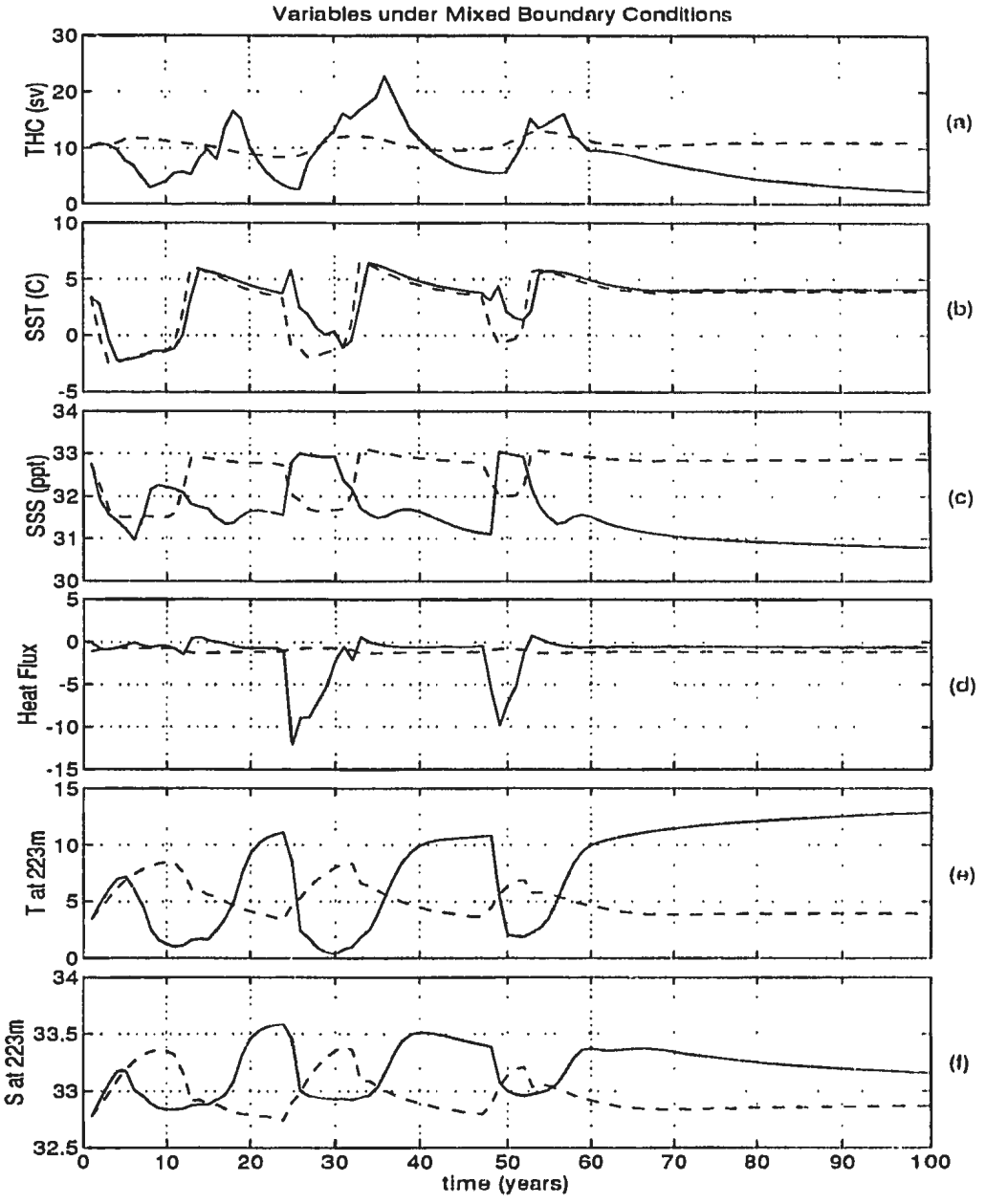

Figure 4.11: Variables under mixed boundary conditions (restoring time = 10 days). (a) Maximum thermohaline circulation; (b) surface temperature; (c) surface salinity; (d) implied surface heat flux; (e) temperature at 223 m; and (f) salinity at 223 m. All but (a) are for a point at 43.2°E, 57.8°N. Solid lines are for mixed boundary conditions and dashed lines are for the control run.

reduces in the warming phase under mixed boundary conditions, in contrast to what happens in the control run. On the other hand, when the surface temperature in the data is going down, surface heat-loss is enhanced and the freshwater is mixed down by the increased deep convection. The freshwater cap is diminished rapidly (Fig. 4.11c) and a violent overturning circulation ("flushes") occurs (Fig. 4.11a), resulting in a large heat loss (Fig. 4.11d).

Though the surface temperature is forced to relax to the control-run data, the sub-surface temperature and salinity are not directly controlled under any of our surface conditions. Under mixed boundary conditions, the sub-surface layers are cooled and freshened when the "flush" events occur (compare (e) and (f) with (a) and (d) in Fig. 4.11). There is no agreement with the control run.

When a restoring boundary condition is applied to the surface salinity as well as the surface temperature, as in the both-restoring boundary condition experiment, the feedback between heat loss reduction and the development of the freshwater cap is broken. The thermohaline circulation is therefore very well simulated. Needless to say both the surface temperature and salinity are correct because of the use of restoring conditions. Sub-surface temperature and salinity are also correct because their values depend on the poleward heat/salt transport (associated with the thermohaline circulation) and vertical mixing with the surface temperature and salinity.

In the reversed mixed boundary condition experiment, the positive feedback between the development of a freshwater cap and heat-loss reduction is extinguished since both the surface heat flux and the surface salinity are now prescribed. Now we analyze what happens to the controlled and uncontrolled variables in this case. This time the surface freshwater flux changes with time since a restoring condition is applied to surface salinity using the time-varying SSS data from the control run. When the surface salinity in the data is going up, a reduction of surface freshwater input occurs and the deep convection process tends to be enhanced. Heat is then lost over a deeper water column, causing warmer surface water. This tendency for surface temperature to increase with increasing surface salinity is a feature of the control run. Note that the warming tendency does not lead to a positive feedback (unlike what happens to the uncontrolled variable, SSS, under mixed boundary conditions) because warming itself will reduce deep convection. On the other hand, when the surface salinity in the data is going down, an increase of surface freshwater input occurs and the deep convection process tends to be reduced. Heat is then lost over a shallower depth, causing colder surface water. Again, this is consistent with what happens in the control run. The cooling tendency does not lead to a positive feedback because cooling will enhance deep convection again. Thus even though surface temperature is not controlled in this case, it still has the correct value.

A common feature of the successful experiments is that all of them have a correct surface heat flux distribution (prescribed or implied, Fig. 4.12), whereas the surface salt flux (Fig. 4.13) may differ. This shows the importance of getting the surface heat flux correct because it is crucial to ensure there is always heat loss at high latitudes in order to prevent the formation of a freshwater cap and guarantee a realistic thermohaline circulation. Getting the thermohaline circulation correct ensures that the sub-surface variables also have the correct values. The results also show that controlling surface salinity is more important than getting every detail of the freshwater flux correct. These results suggest that we can use both-restoring boundary conditions or reversed mixed boundary conditions to simulate interdecadal variations of the thermohaline circulation.

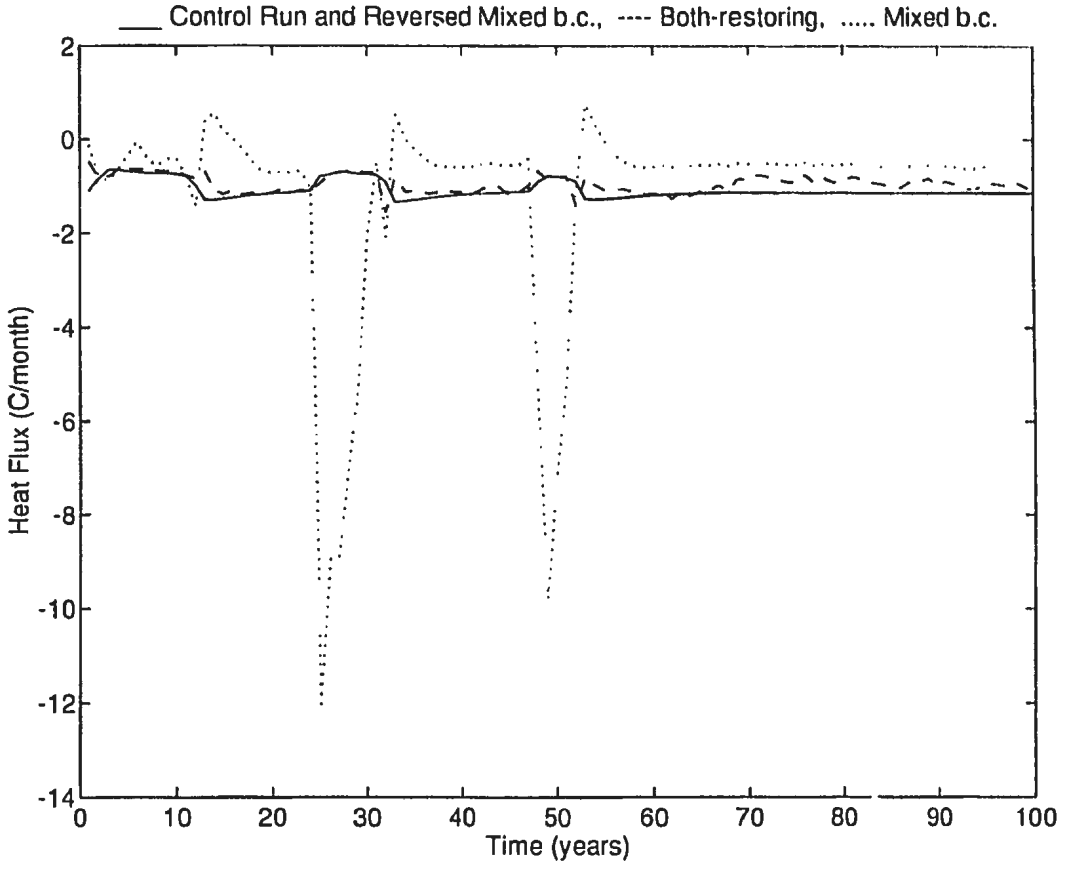

Figure 4.12: Surface heat flux (input or implied) into the ocean under different kinds of boundary conditions: control run and reversed mixed b. c. (solid line); both-restoring b. c. (dashed line); mixed b. c. (dot line). This is for a point at 43.2°E, 57.8°N and a restoring time of 10 days for those cases using restoring conditions.

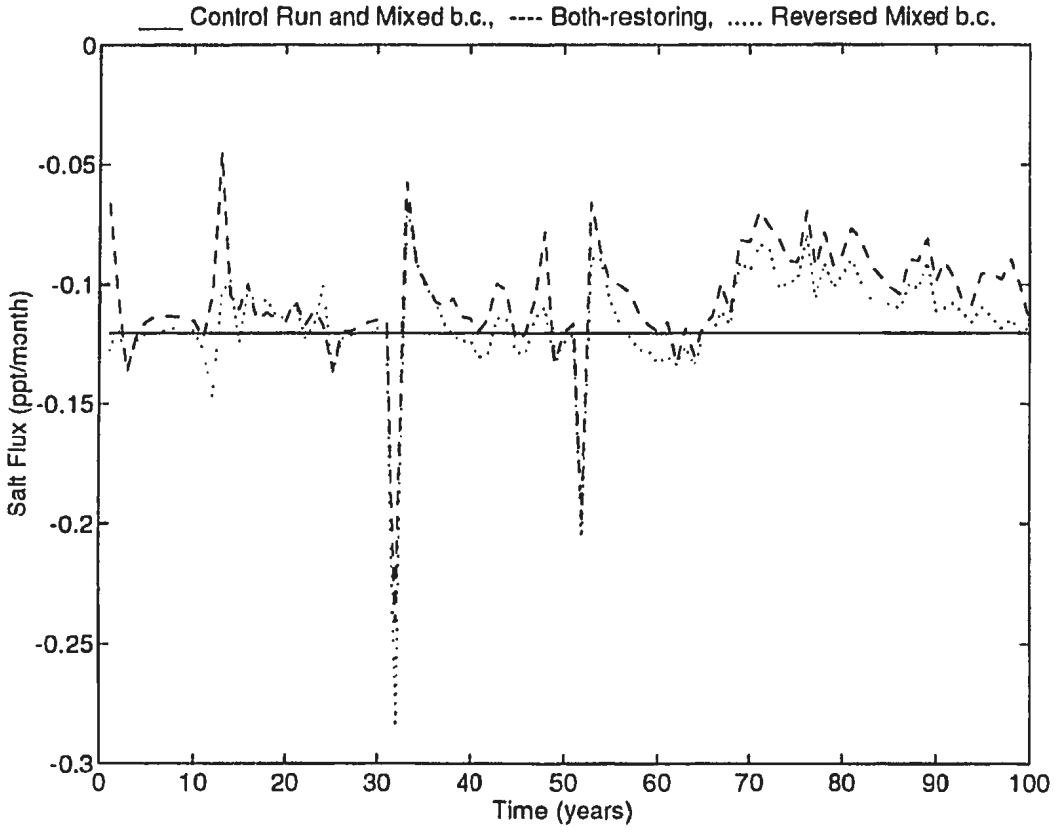

Figure 4.13: Surface salt flux (input or implied) into the ocean under different kinds of boundary conditions: control run and mixed b. c. (solid line); both-restoring b. c. (dashed line); reversed mixed b. c. (dot line). This is for a point at 43.2°E, 57.8°N and a restoring time of 10 days.

Chapter 5

Summary and Conclusion

Observation shows that temperature and salinity in the North Atlantic have decadal and interdecadal variations [Lazier ((1980), Levitus (1989)a,b,c, Dickson *et al.* (1988), Read and Gould (1992)] and there is evidence which supports the idea that these variations are associated with changes in ocean circulation [Bjerknes (1964), Bryan and Stouffer (1991), Kushnir (1993), Delworth *et al.* (1993) and Deser and Blackmon (1993), Greatbatch and Xu (1993)]. Motivated by this, we try to develop strategies to simulate decadal or interdecadal variations of the ocean thermohaline circulation through an Ocean General Circulation Model (OGCM) using decadally-varying surface data. We do this in an idealized North Atlantic sized box geometry before going on to the complexities of attempting realistic simulations using real data in

future research. We experiment with different kinds of boundary conditions at the ocean surface to test the behavior of the model in order to determine what surface data are appropriate for this purpose. We do this because there is a desire to use surface temperature and salinity data, since compared to flux data, they are more accurate and more readily available. The natural way to drive the ocean is to use the surface heat and freshwater fluxes. Unfortunately data on these fluxes are too uncertain and sparse.

The ocean model we use is very similar to the well-known Bryan-Cox-Semtner model. In order to determine what surface data is needed to drive the model, we first reproduced the results described by Zhang, Greatbatch and Lin (1993). They found that when a zero-heat-capacity atmosphere is coupled to the ocean model, a cold, fresh water pool is developed and advected horizontally and vertically by the circulation in high latitudes, showing decadal time-scale oscillations. Temperature, salinity, surface heat and freshwater flux are output from this control run and serve as "observations" in the further experiments.

To simulate the interdecadal variations with the "observations" (i.e. data from the control run), four kinds of surface boundary conditions are used: i) both-flux boundary conditions, in which the time-dependent heat flux and freshwater flux data are imposed on the ocean surface; ii) both-restoring boundary conditions, in which

temperature and salinity at the top model level are restored to the time-dependent SST and SSS data, respectively; iii) mixed boundary conditions, in which the top-level temperature is restored to the time-dependent SST data, while a flux boundary condition is applied to salinity; and iv) "reversed mixed" boundary conditions, in which the top-level salinity is restored to time-dependent SSS while the time-dependent surface heat flux is used to provide the surface boundary condition for temperature.

The experiments show that all the choices work well except mixed boundary conditions. It is found that a correct simulation of the thermohaline circulation is necessary for a realistic distribution of the sub-surface variables. Under mixed boundary conditions there is a positive feedback between the development of a freshwater cap and heat-loss reduction, resulting in either a collapsed or violent overturning thermohaline circulation, in contrast to what happens in the control run. So mixed boundary conditions are not suitable for our purpose to simulate interdecadal variations. Both-restoring boundary conditions break this feedback by controlling the surface salinity. This guarantees a correct deep convection and thermohaline circulation and consequently a correct distribution of the sub-surface temperature and salinity. In contrast with mixed boundary conditions, reversed mixed boundary conditions do not allow a freshwater cap to grow either because both the surface heat flux and the surface salinity are controlled.

A common feature of the successful experiments is that all of them have a correct surface heat flux distribution (prescribed or implied), whereas the surface freshwater flux may defer (though not significantly). This shows that whatever the boundary condition, it is necessary to get the surface heat flux seen by the ocean correct in order to have a realistic thermohaline circulation. It also shows that controlling surface salinity is more important than getting every detail of the freshwater flux correct (fortunately, freshwater flux data are the poorest). These results show that we should use both-restoring boundary conditions or reversed mixed boundary conditions to simulate interdecadal variations of the thermohaline circulation.

Bibliography

Bjerknes, J., 1964: Atlantic air-sea interaction. *Adv. Geophys.*, **10**, 1-82.

Bretherton, F. P., 1982: Ocean climate modeling. Progress in Oceanography, Vol. 11, Pergamon, 93-129.

Bryan, F., 1986a: Maintenance and variability of the thermohaline circulation. Ph.D. thesis, Atmospheric and Oceanic Sciences Program, Princeton University, 254pp.

———, 1986b: High-latitude salinity effects and interhemospheric thermohaline circulations. *Nature*, **323**, 301-304.

Bryan, K., 1969: A numerical method for the study of the circulation of the world ocean. *J. Comput. Phys.*, **4**, 347-376.

Bryan, K., 1984: Accelerating the convergence to Equilibrium of Ocean climate model. *J. Phys. Oceanogr.*, **14**, 666-673.

Bryan, K., and R.J. Stouffer, 1991: A note on Bjerknes' hypothesis for North Atlantic variability. *J. Mar. Res.*, **1**, 229-241.

Clarke, R. A., 1992: Global warming, ocean cooling. *Nature*, **360**, 17-18.

Courant, R., Friedrichs, K. and Lewy, H., 1928: Über die partiellen Differenzengleichungen der mathematischen Physik. *Math. Annalen*, **100**, 32-74.

Cox, M.D., 1984: A primitive equation, 3-dimensional model of the ocean. GFDL Ocean Group Technical Report No. 1, GFDL/Princeton University, USA.

Delworth, T., S. Manabe, and R.J. Stouffer, 1993: Interdecadal variations of the thermohaline circulation in a coupled ocean-atmosphere model. *J. Climate*, in press.

Deser, C., and M.L. Blackmon, 1993: Surface climate variations over the North Atlantic Ocean during winter: 1900-1989. *J. Climate*, **6(9)**, 1743-1753.

Dickinson, R. E., 1981: Convergence rate and stability of ocean-atmosphere coupling schemes with a zero-dimensional climate model. *J. Atmos. Sci.*, **38**, 2112-2120.

Dickson, R.R., J. Meinke, S.-A. Malmberg and A.J. Lee, 1988: The great salinity anomaly in the northern North Atlantic, 1968-1982. *Prog. Oceanogr.*, **20**, 103-151.

Ghil, M., and R. Vautard, 1991: Interdecadal oscillations and the warming trend in global temperature time series. *Nature*, **350**, 324-327.

Gordon, A.L., 1986: Interocean exchange of thermocline water. *J. Geophys. Res.*, **91(C4)**, 5037-5046.

Gordon, A.L., S.E. Zebiak and K. Bryan, 1992: Climate variability and the Atlantic Ocean. *EOS*, **73(15)**, 161-165.

Greatbatch, R.J., A.F. Fanning, A.G. Goulding and S. Levitus, 1991: A diagnosis of interpentadal circulation changes in the North Atlantic. *J. Geophys. Res.*, **96 C(12)**, 22,009-22,023.

Greatbatch, R.J., and J. Xu, 1993: On the transport of volume and heat through sections across the North Atlantic: climatology and the pentads 1955-59, 1970-74.*J. Geophys. Res.*, **98 C(6)**, 10,125-10,143.

Greatbatch, R.J., and S. Zhang, 1993: An interdecadal oscillation in an idealized ocean basin forced by constant heat flux. *J. Climate*, submitted.

Haney, R. L., 1971: Surface thermal boundary condition for ocean circulation models. *J. Phys. Oceanogr.*, **1**, 241-248.

Huang, R. X., 1993: Real freshwater flux as a natural boundary condition for the salinity balance and thermohaline circulation forced by evaporation and precipitation. *J. Phys. Oceanogr.*, **23**, 2428-2446.

Kushnir, Y., 1993: Interdecadal variations in North Atlantic sea surface temperature and associated atmospheric conditions. *J. Climate*, in press.

Lazier, J.R.N., 1980: Oceanographic conditions at Ocean Weather Ship *Bravo*, 1964-1974. *Atmosphere-Ocean*, **18**, 227-238.

Levitus, S., 1989a: Interpentadal variability of temperature and salinity at intermediate depths of the North Atlantic Ocean, 1970-1974 versus 1955-1959. *J. Geophys. Res.*, **94(C5)**, 6091-6131.

- -, 1989b: Interpentadal variability of salinity in the upper 150m of the North Atlantic Ocean, 1970-1974 versus 1955-1959. *J. Geophys. Res.*, **94(C7)**, 9679-9685.

-, 1989c: Interpentadal variability of temperature and salinity in the deep North Atlantic, 1970-1974 versus 1955-1959. *J. Geophys. Res.*, **94(C11)**, 16125-16131.

Manabe, S., and R. J. Stouffer, 1988: Two stable equilibria of a coupled ocean-atmosphere model. *J. Climate*, **1**, 841-866.

Marotzke,J., 1989: Instabilities and steady states of the thermohaline circulation. *Oceanic Circulation Models: Combining Data and Dynamics*, D. L. T. Anderson and J. Willebrand, Eds., Kluwer, 501-511.

———, 1990: Instabilities and multiple equilibria of the thermohaline circulation. Ph.D. thesis, Ber.Inst.Meeresk.Kiel, 194, 126pp.

———, 1991: Influence of convective adjustment of the stability of the thermohaline circulation. *J. Phys. Oceanogr.*, **21(6)**, 903-907.

Read, J.F., and W.J. Gould, 1992: Cooling and freshening of the subpolar North Atlantic Ocean since the 1960's. *Nature*, **360**, 55-57.

Sarkisyan, A. S. and V. F. Ivanov, 1971: Joint effect of baroclinicity and bottom relief as an important factor in the dynamics of sea currents. *Izvestiya of the Academy of the Sciences of the U.S.S.R. Atmospheric and Oceanic Physics*, **7**, 173-188.

Sato, O.T. and T. Rossby, 1993: Seasonal and secular variations in dynamic height anomaly and transport of the Gulf Stream. Graduate School of Oceanography, University of Rhode Island, Kingston, RI, 02881, USA.

Schmitt, R. W., P. S. Bogden and C. E. Dorman, 1989: Evaporation Minus Precipitation and Density Fluxes for the North Atlantic. *J. Phys. Oceanogr.*, **19**, 1208-1221.

Schopf, P. S., 1983: On equatorial waves and El Niño. II: Effects of air-sea thermal coupling. *J. Phys. Oceanogr.*, **13**, 1878-1893.

Semtner, A.J., 1974: An oceanic general circulation model with bottom topography. *Numerical Simulation of Weather and Climate*, Tech.Rept.No.9, Department of Meteorology, University of California, Los Angeles, 99pp.

Tziperman, E. and K. Bryan, 1993: Estimating global air-sea fluxes from surface properties and from climatological flux data using an oceanic general circulation model. *J. Geophys. Res.*, in press.

Weaver, A.J. and E.S. Sarachik, 1991a: The role of mixed boundary conditions in numerical models of the ocean's climate. *J. Phys. Oceanogr.*, **21(9)**, 1470-1493.

Weaver, A.J. and E.S. Sarachik, 1991b: Evidence for Decadal Variability in an ocean general circulation model: An advective mechanism. *Atmosphere-Ocean*, **29(2)**, 197-231.

Zhang, S., R.J. Greatbatch and C.A. Lin, 1993a: A re-examination of the polar halocline catastrophe and implications for coupled ocean-atmosphere models. *J. Phys. Oceanogr.*, **23(2)**, 287-299.